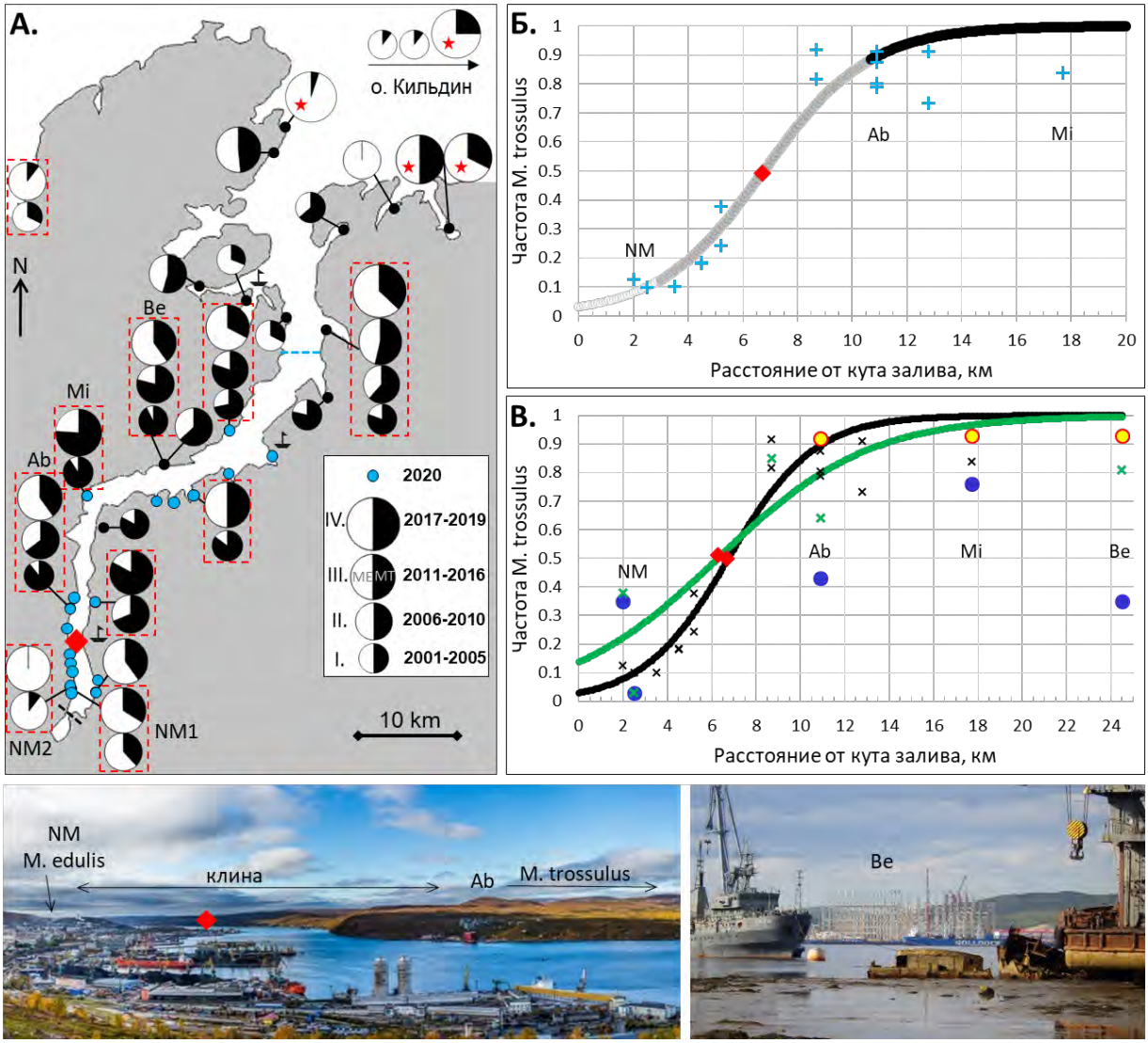

Рис 1.1.1. Структура и динамика гибридной зоны между Mytilus edulis и M. trossulus в Кольском заливе Баренцева моря, по нашим данным 2001-2000 гг. На всех иллюстрациях аббревиатуры – названия мест сбора, красный ромб – центр клины в вершине залива. А. Карта-схема района. Диаграммы показывают вклад генов M. edulis (белый сектор) и M. trossulus (чёрный), оцененный по3-4 локусам, в структуру выборок. Размеры диаграмм отражают период сбора материала (см. легенду). Выборки разных лет сбора из одних и тех же мест обведены рамкой. Звёздами отмечены новые выборки 2019 г. сбора. Голубые точки – места сбора в июле-августе 2020 года. Чёрная пунктирная линия показывает мост через р. Тулома (условная граница река/море). Б. Доля M.trossulus в выборках 2020 г. как функция от расстояния от Туломы, км. Крестики - эмпирические оценки, по морфологическим данным. Линия - предсказанные моделью S-образной клины частоты M. trossulus. Белый участок линии – абсолютное доминирование M. edulis, черный - M. trossulus, серый – клина. В. Структура популяций вершины залива в разные периоды. Жёлтые точки – частоты M. trossulus в первом периоде наблюдений, зеленые – во втором, синие – в третьем, черные – в 2020 г. Черная линия – клина в 2020 г., зелёная – во втором периоде. Видно, что при изменении формы клины во времени ее центр не изменился. Фотографии. Слева. Панорама южного колена Кольского залива, вид от подножия памятника «Защитникам Советского Заполярья в годы ВОВ». Показан р-н клины. Справа: вид на точку Be (Белокаменка), места строительства Центра строительства крупнотоннажных морских сооружений НОВАТЭК, с противоположного берега залива.

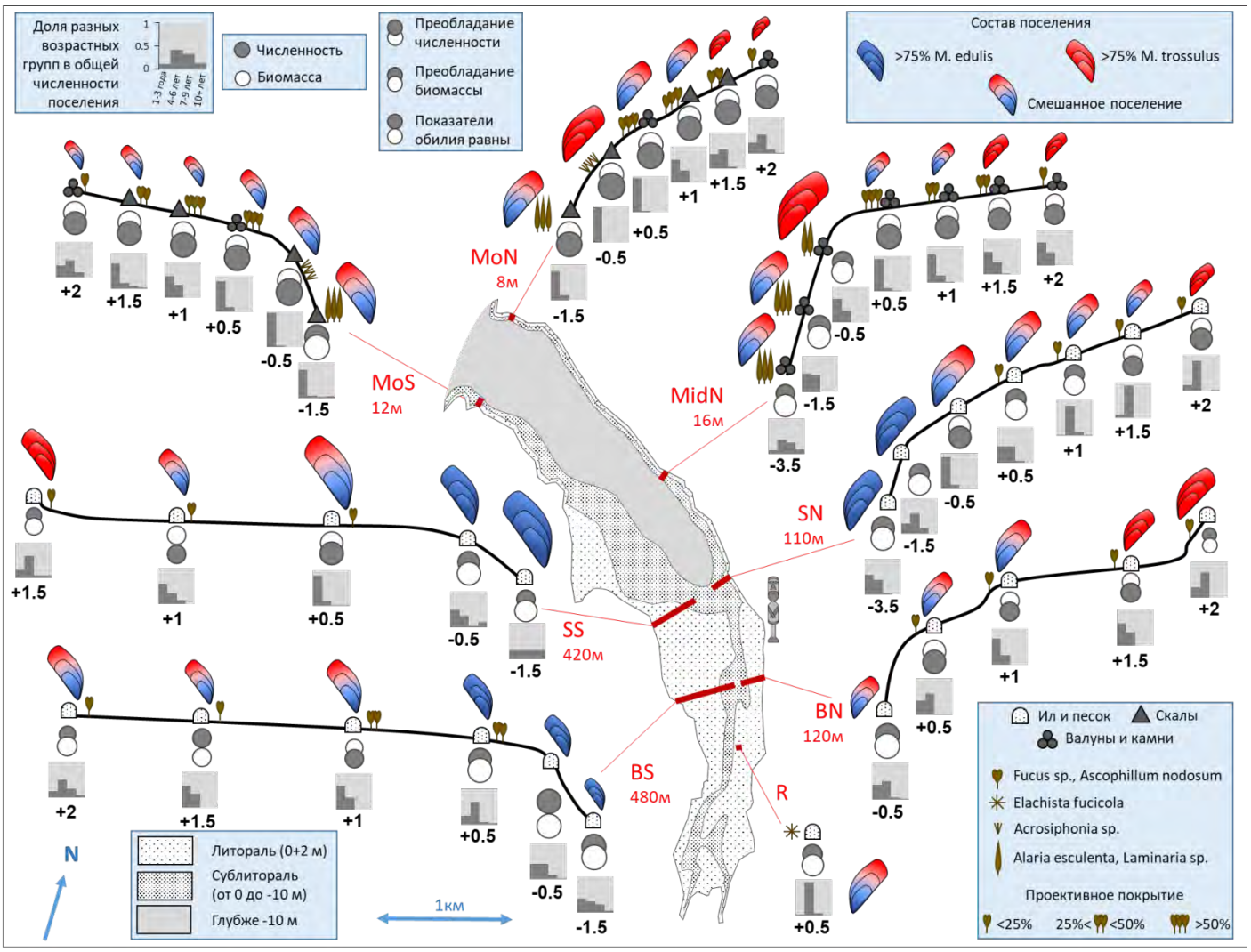

рис. 1.1.2.1. Характеристика поселений мидий Mytilus edulis и M. trossulus в губе Тюва в 2009-2010 гг. В центре - карта-схема губы, показана батиметрия. Красные линии на схеме – вертикальные разрезы через зону, населенную мидиями, на которых проводили исследование. Красным даны названия разрезов и их протяженность в м. Черные линии – схематические профили разрезов. Приведены характеристики биотопов (тип субстрата, доминирующие виды макрофитов и их проективное покрытие) (см. легенду). Указаны глубины сбора мидий, от «0» глубин. Для каждого поселения приведена информация об обилии, возрастной структуре, размерах раковин и таксономическом составе (см. легенду). Крупная мидиевая банка расположена в куту губы, в сублиторали и на нижней литорали в районе разрезов BN, BS, SS и SN.

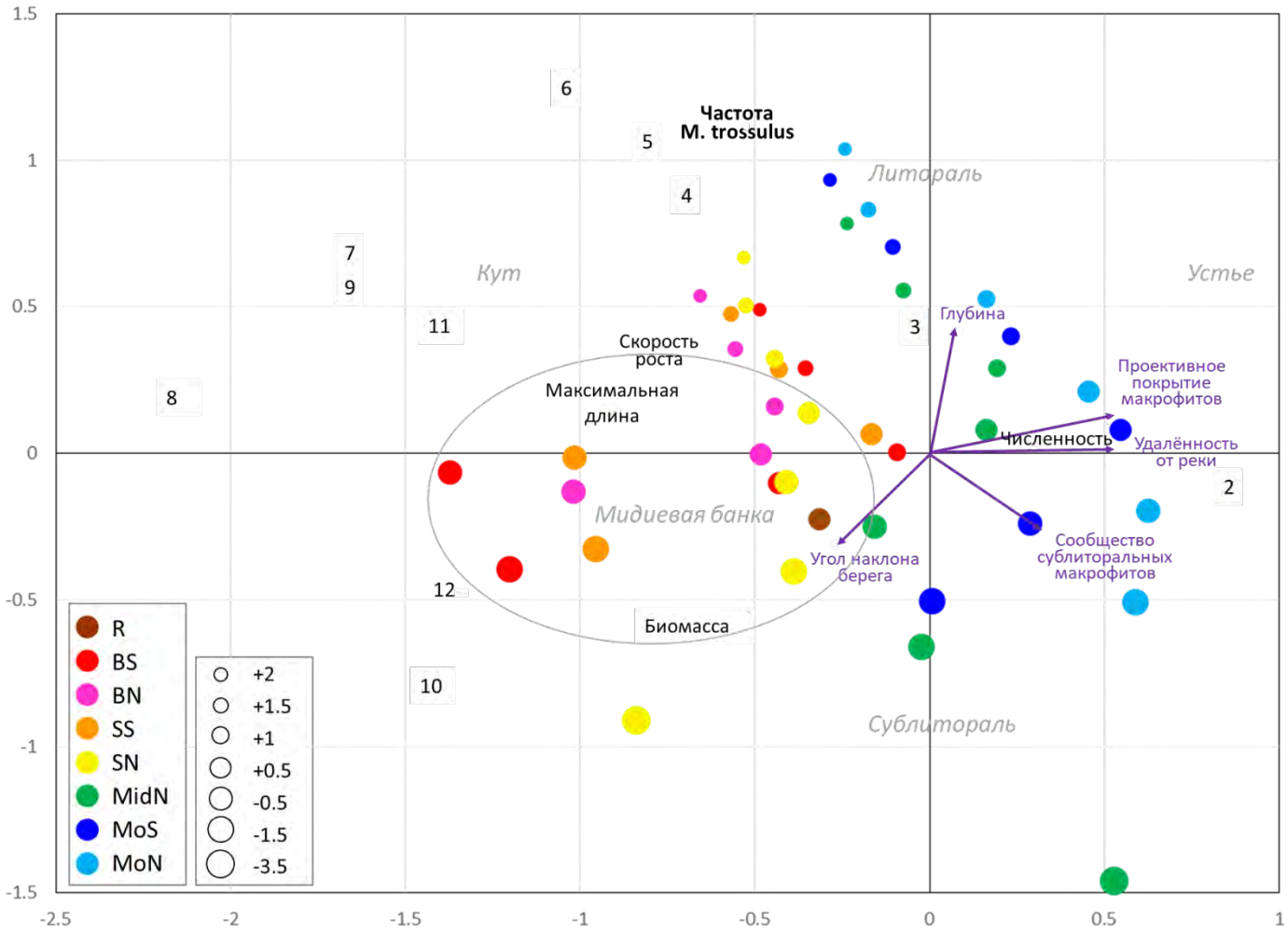

Рис. 1.1.2.2**.** Поселения мидий губы Тюва в 2009-10 гг. в пространстве канонических осей. Объектами ординации выступали поселения (точки на графике, цвет отражает разрез как на рис. 1.1.2.1., размер пропорционален глубине обитания), каждое из которых было описано уникальным набором популяционных характеристик (численность, биомасса, средний возраст, максимальная наблюдаемая длина раковины, интегральный показатель скорость роста, частота M. trossulus), а в качестве предикторов (внешних переменных) выступали характеристики местообитаний (расстояние от устья реки, угол наклона берега, проективное покрытие макрофитов, наличие/отсутствие сообщества сублиторальных макрофитов). На графике приведены популяционные характеристики и предикторы, значимо влияющие на ординацию. Серым курсивом даны выделы губы, куда попадают точки. Первая каноническая ось «делит» местообитания на «устьевые» и «кутовые». Первые характеризуются более высокой численностью и преобладанием молоди. Вторая ось связана с глубиной. Доля M. edulis возрастает с глубиной. Выборки с мидиевой банки в куту губы группируются в левом нижнем квадранте (высокая биомасса, дефицит молоди, большие размеры мидий, доминирование M. edulis, ср. с рис. 1.1.2.1).

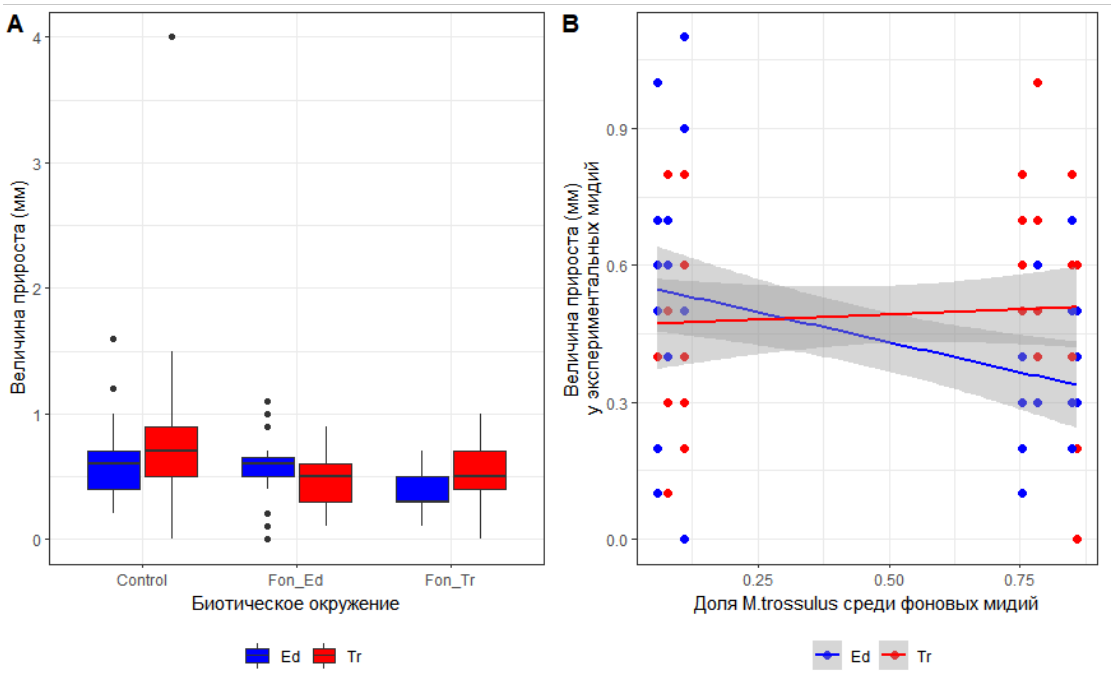

Рис 1.2. Скорость роста мидий M.edulis и M.trossulus в экспериментальных поселениях, в зависимости от плотности и таксономического состава поселений. Мидии содержались 2 месяца в 12 садках стандартного размера 1500 кубических см. В каждом садке содержалось по 10 индивидуально меченых «экспериментальных» M. edulis и M. trossulus. 4 садка были контрольными (только «экспериментальные» мидии; «control» на графиках). В 4 садках вместе с «экспериментальными» содержалось по 150 мидий из популяции с абсолютным доминированием M. trossulus (Fon_Tr). Еще в 4 садках вместе с «экспериментальными» содержалось по 150 мидий из популяции с абсолютным доминированием M. edulis (Fon_ed). А. Боксплоты, отражающие распределение величин прироста раковин «экспериментальных» M. edulis (Ed) и M. trossulus (Tr) в разных садках. Большие значения прироста в контроле объясняются низкой плотностью поселения. В. Линии регрессии, описывающие величину прироста «экспериментальных» M. edulis (Ed) и M. trossulus (Tr) в зависимости от доли *M. trossulus в поселениях*. В садках с абсолютным доминированием *M. trossulus* величина прироста M. edulis значимо ниже (параметры линейной модели приведены в таблице +.1).

Табл. 1.2. Параметры линейной модели, описывающей величину прироста M. edulis и M. trossulus в экспериментальных поселениях, в зависимости от таксономического состава поселений.

Член модели	Параметр	SE	t	p.value
(Intercept)	0.358	0.308	1.162	0.248
Доля M.trossulus (PT)	-0.280	0.090	-3.101	0.002 **
Вид(Tr)	-0.092	0.073	-1.257	0.211
Начальный размер (L)	0.011	0.017	0.673	0.502
PT:Вид(Tr)	0.320	0.123	2.590	0.011 *

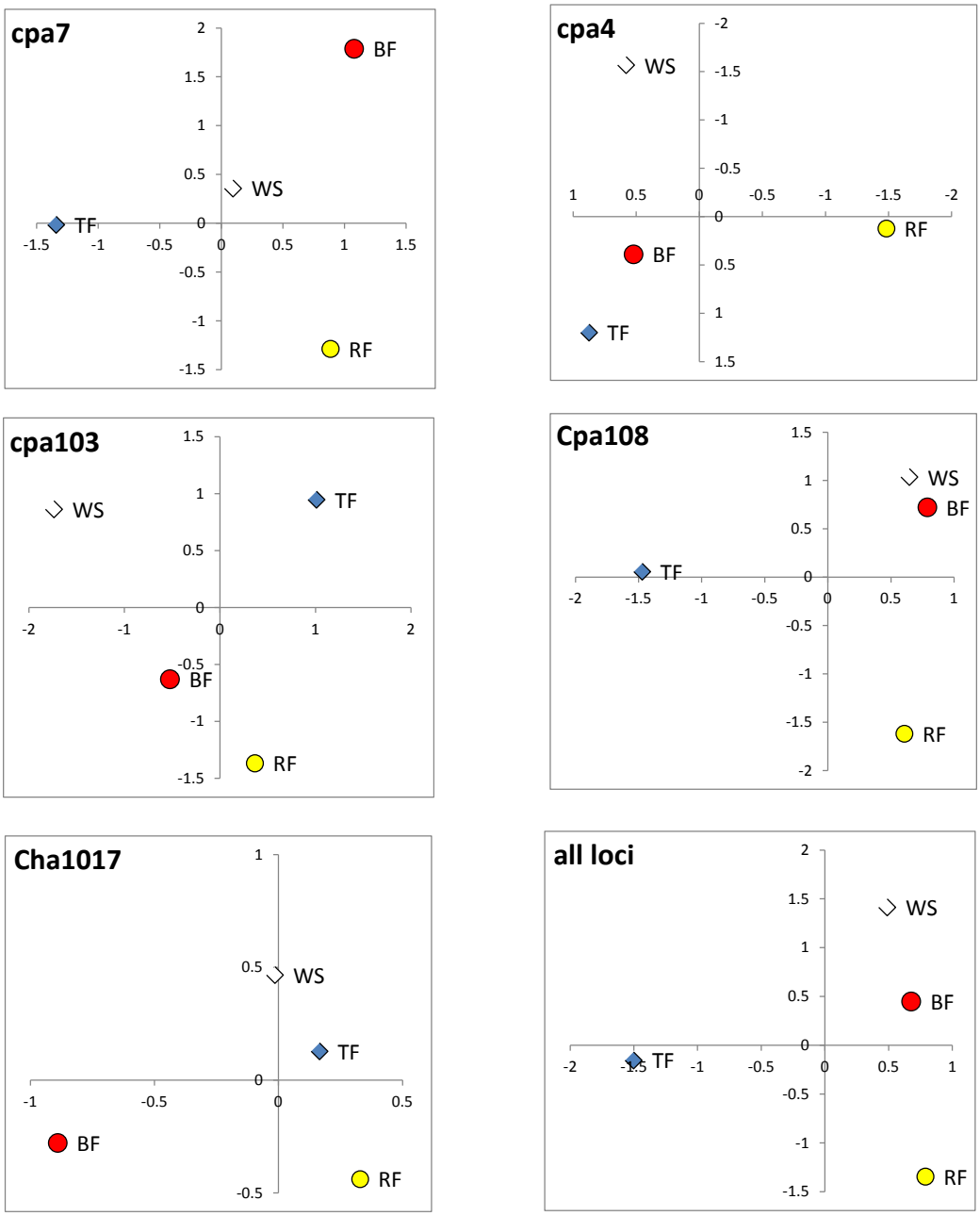

Рис. 1.3.1. Генетические особенности популяций морских сельдей (Clupea pallasii, C. harengus) норвежских фиордов. Ординация (анализ корреспонденций) выборок из Россфиорда (RF), Балсфиорда (BF), Трондхеймфиорда (TF) и Кандалакшского залива Белого моря (WS) по частотам аллелей микросателлитных локусов. Приведены названия локусов; график all loci – анализ по всем локусам. Оси на графиках ориентированы таким образом, чтобы выборка RF попадала в один и тот же квадрант. Средний объем выборки – 18 особей.

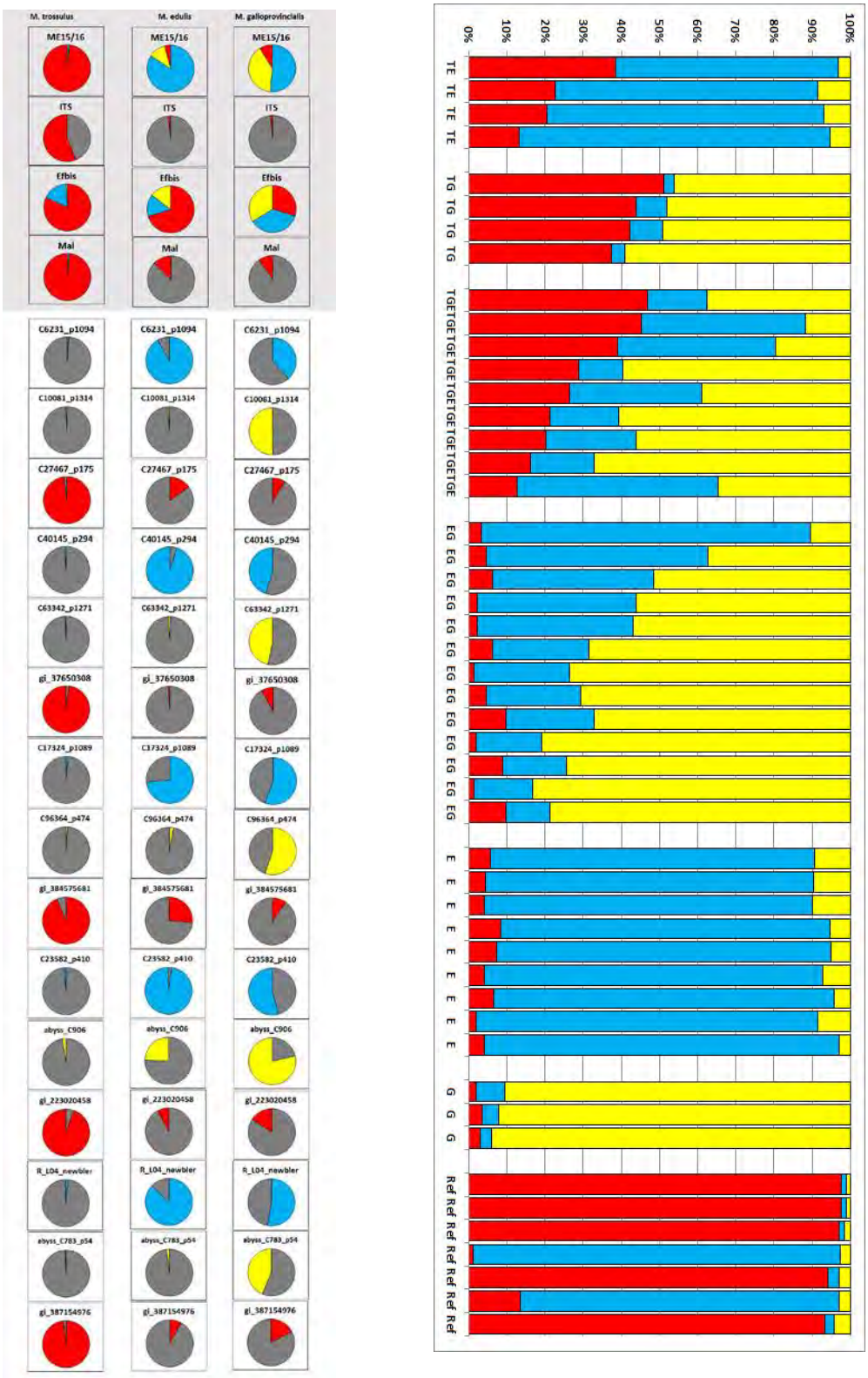

Рис. 1.3.2. Генетическая структура выборки мидий Mytilus из Гасейд, выявляемая методом Structure. Циклограммы - частоты видоспецифических аллелей M.edulis (синий сектор), M. trossulus (красный) и M. galloprovincialis (желтый) в трех выявленных кластерах (у трех «видов»). Вертикальные ряды – кластеры, горизонтальные – локусы. Из 19 маркеров верхние четыре - традиционные (ПЦР+рестрикция), остальные – SNP. Столбчатая диаграмма – вклад генов трех кластеров («видов» - M.edulis - синий сектор, M. trossulus – красный, M. galloprovincialis - желтый) в генотипы особей. В анализ включены 42 мидии из Гасейд (на графике сортированы на группы «чистопородных» и разных гибридов) и 7 из других популяций (самые нижние на графике).

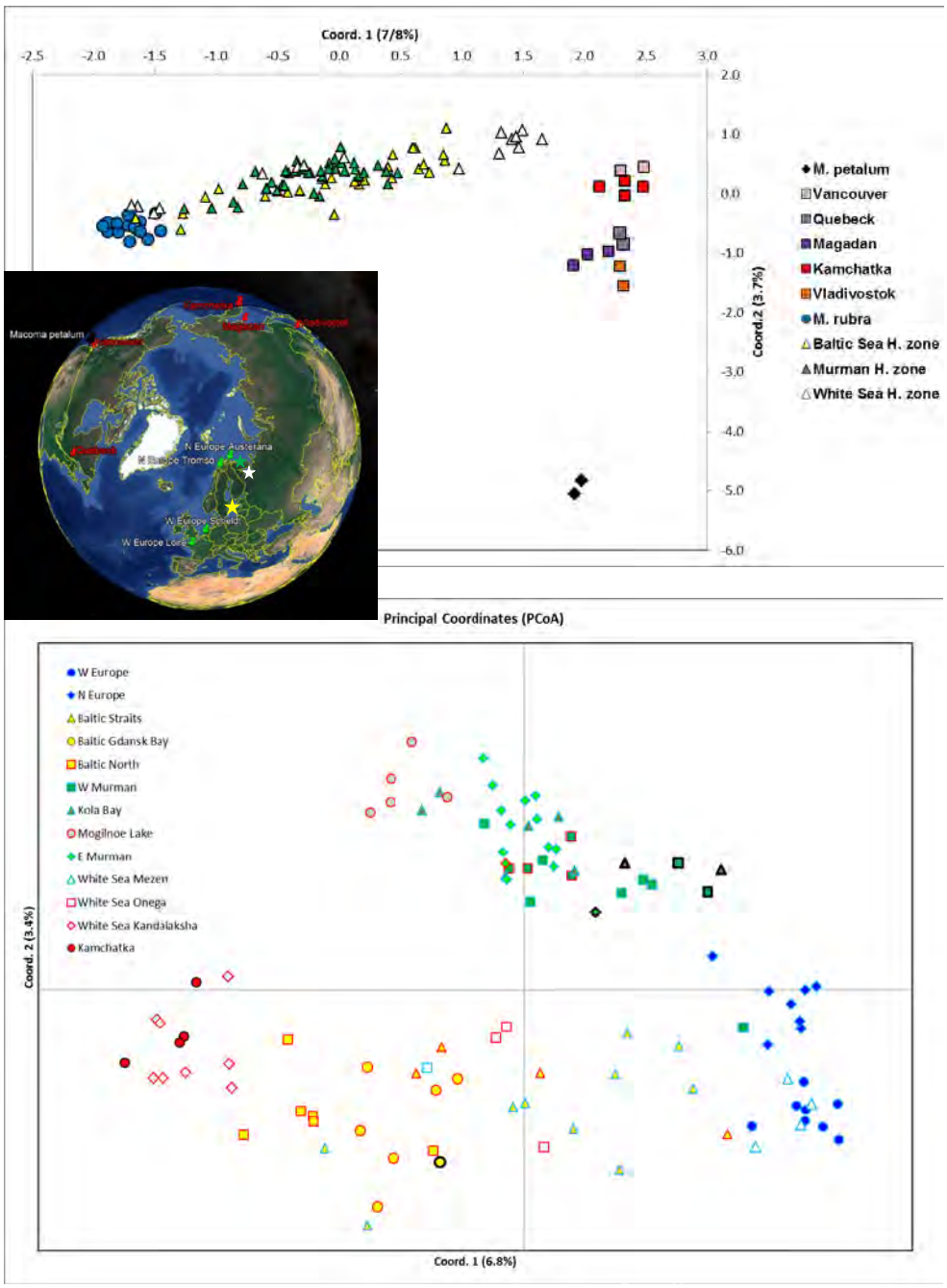

Рис. 2.1.1. Анализ географической изменчивости у балтийских ракушек Macoma petalum, Limecola balthica и L. rubra по маркерам SNP, выявленным в транскриптомах особей. PCoA ординация (кодоминантные генетические расстояния) мультилокусных генотипов из популяций Тихого, Атлантического и Северного ледовитого океанов (вверху, 1819 SNP) и, отдельно, - из европейских популяций и с Камчатки (внизу, 1319 SNP). Особи из разных географических популяций даны значками разного цвета и формы. На нижнем – «европейском» графике цвет контура значка отражает митохондриальный генотип особи: красный - L. balthica, синий - L. rubra, черный жирный - предположительно, оба видовых генома. На карте «пинами» показаны места сбора «чистопородных» L. balthica, M. petalum и L. rubra, звездочками – три района, где обнаружена L. balthica (гены этого вида) и гибридизация между L. balthica и L. rubra в Европе. Эти районы -Балтийское море (Baltic Sea H. zone на карте, желтые значки на графиках) Кольское побережье Баренцева моря (Murman H. Zone, разные оттенки зеленого) - и Белое море (White Sea H. zone, белые).

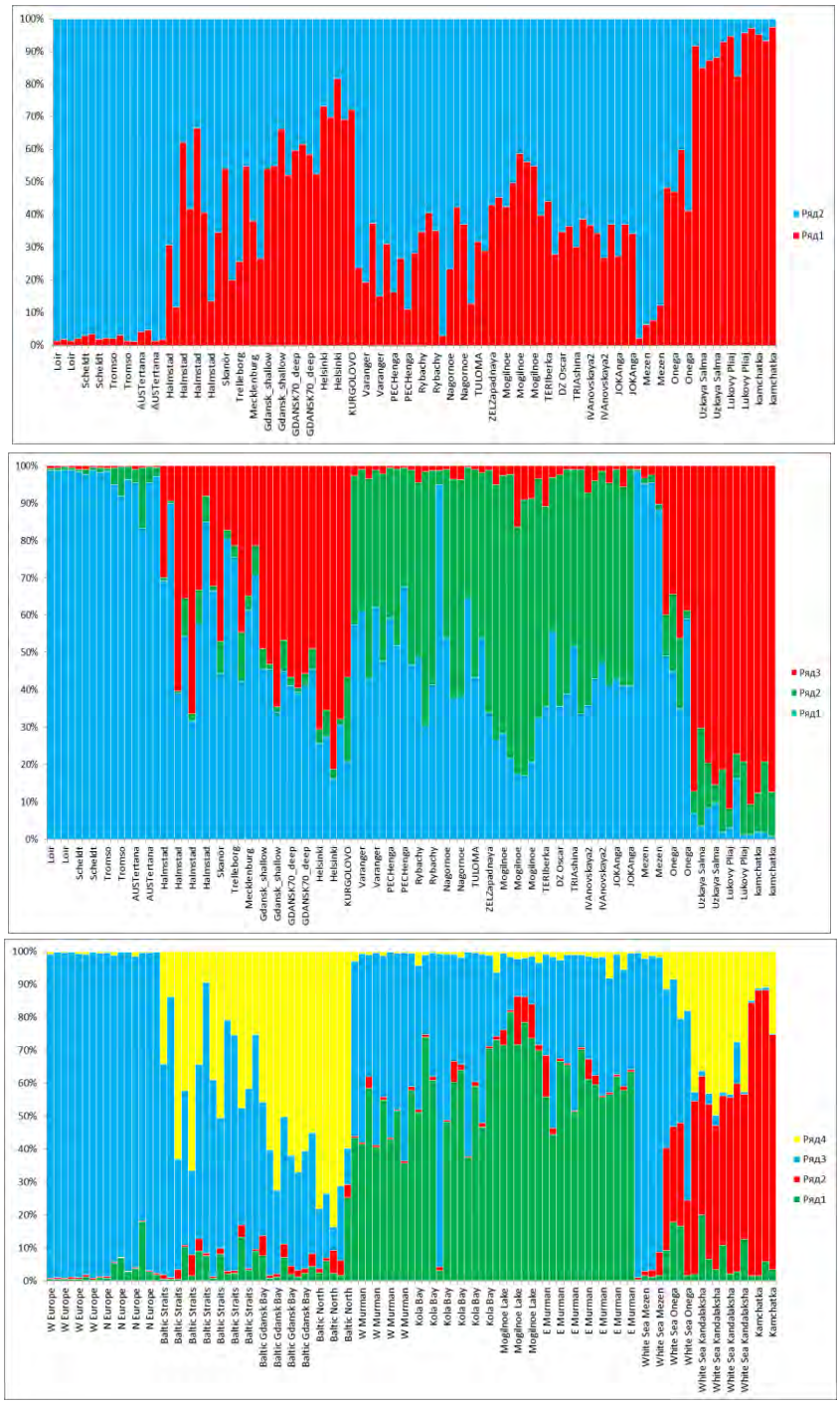

Рис. 2.1.2. Анализ популяционной географической изменчивости и гибридизации у балтийских ракушек Limecola balthica и L. rubra в Европе по 1319 маркерам SNP, выявленным в транскриптомах особей. Кластеризация генотипов методом Structure в рамках моделей с числом кластеров от двух (вверху) до четырех (внизу). Те же данные, что на предыдущем рисунке. Включена выборка из вод Камчатки, как референсы L. balthica. На нижнем графике подписи как на предыдущем рисунке, на верхних графиках указаны конкретные места сбора. Выборки из гибридных зон расположены закономерно: в Балтике от Датских проливов к северным заливам, на Мурмане с запада на восток. Метод различает генофонды L. balthica и L. rubra (верхний график) и находит отличия между балтийской, мурманской и беломорской гибридными линиями ракушек (нижние графики).

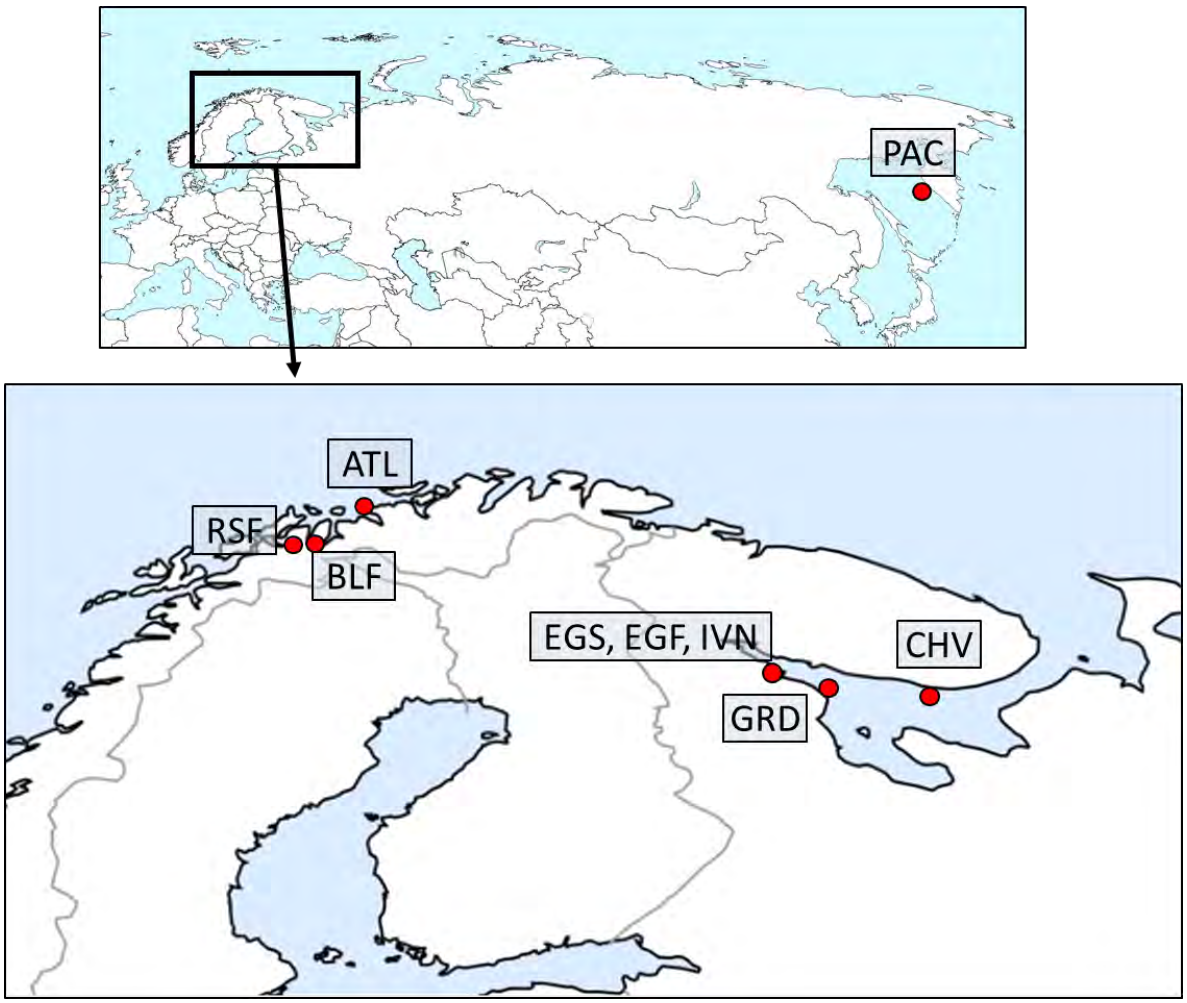

Рис. 3.1.1. Карта-схема района исследования. Отмечены места сбора материала. Названия выборок как в табл. 3.1.1.

Место сбора	Сокращенное название	Дата сбора	Location	Объем выборки, N	Средняя длина тела (SL+- SE)	Число позвонков	Популяционная характеристика	Материал для генетического анализа	Генетическая характеристика	доля тихоокеанских генов
Норвежское море	ATL	18.01.2019	70°06,15'N, 21°11,00' E	33	27,98±0,51		Типичная атлантическая форма	Имеется от тех же особей	Атлантическая сельдь - 0% С.р.	0
Охотское море	PAC	10.06.2019	53,988N, 1556864E	33	26,36±0,51	52,15(51-54)	Типичная тихоокеанская форма	Планируется получить от этой популяции (Охотское море)	Тихоокеанская сельдь - 100% С.р.	100
Норвежское море, Балсфьорд	BLF		69,3599N, 19,1329E	31	22,24±0,34	53,58(52-55)	Озерная гибрилная форма	Выборка изучена ранее (Laakkonen et al., 2015)	mt - 79% С.р., allozymes - 80% С.р. (Laakkonen), 78% (lit)	79
Норвежское море, Россфьорд	RSF	01.11.2014	69,3046N, 18,2412	32	17,10±0,22	53,86(52-55)	Озерная гибрилная форма	Выборка изучена ранее (Laakkonen et al., 2015)	mt - 50% С.р., allozymes - 50% С.р. (литература)	50
Белое море, Кандалакшский залив, губа Чупа (Левин Наволок)	EGS	15.04.1990	66,3009N, 33,4648E	38	21,66±0,24		Нерест в апреле, низкий темп роста	Эта популяция изучена ранее (Laakkonen et al., 2015)	mt - 96% С.р., allozymes - 95,5% С.р. (литература), 97,4% (Laakkonen)	96,225
Белое море, Кандалакшский залив, губа Чупа (Левин Наволок)	EGF	15.04.1990	66,3009N, 33,4648E	20	24,51±0,49		Нерест в апреле, высокий темп роста	Отсутствует	Скорее всего, как у EGS	96,225
Белое море, Кандалакшский залив, губа Чупа (Левин Наволок)	IVN	26.05.1989 20.06.1989	66,3009N, 33,4648E	40	24,74±0,35		Нерест в июне, высокий темп роста	Эта популяция изучена ранее (Laakkonen et al., 2015)	mt - 89% С.р., allozymes - 93% С.р. (литература), 95,5% (Laakkonen)	91,625
Белое море, Бассейн, Гридино	GRD	02.06.1990	65,9197N, 34,6995E	33	25,73±0,41		Нерест в июне, высокий темп роста	Отсутствует	Скорее всего, как у IVN	91,625
Белое море, Бассейн, Чаваньга	CHV	08.06.1990	66,1061N, 37,7944E	33	27,70±0,48		Нерест в июне, высокий темп роста	Отсутствует	Скорее всего, как у IVN	91,625

Таб. 3.1. Характеристики выборок, использованных в исследовании

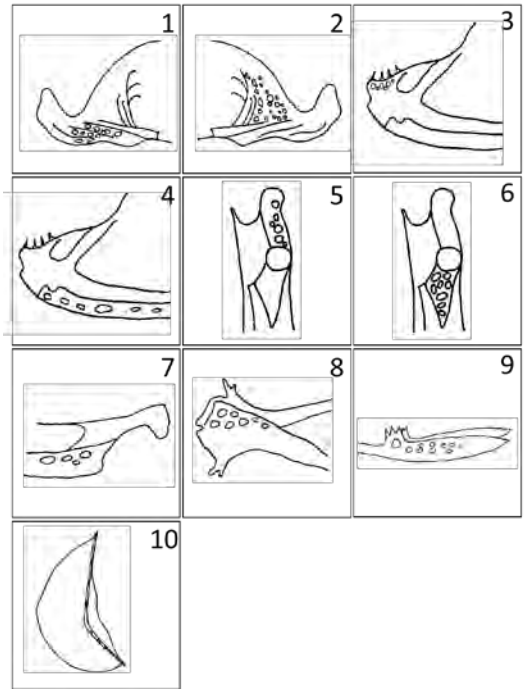

Рис. 3.1.2. Признаки костей черепа, использованные в работе. Описание: 1 – число пор на наружной поверхности articulare, 2 – число пор на внутренней поверхности articulare, 3 – число пор в верхней части наружной поверхности dentale, 4 – число пор в нижней части наружной поверхности dentale, 5, 6 – число пор на указанных участках hyomandibulare, 7 – число пор вдоль всей внутренней поверхности maxillare в ее нижней части, 8 – число пор на указанной поверхности mesethmoideum (на одной стороне кости), 9 – число пор в задней части parasphenoideum (на одной стороне кости), 10 – число пор на praeoperculum.

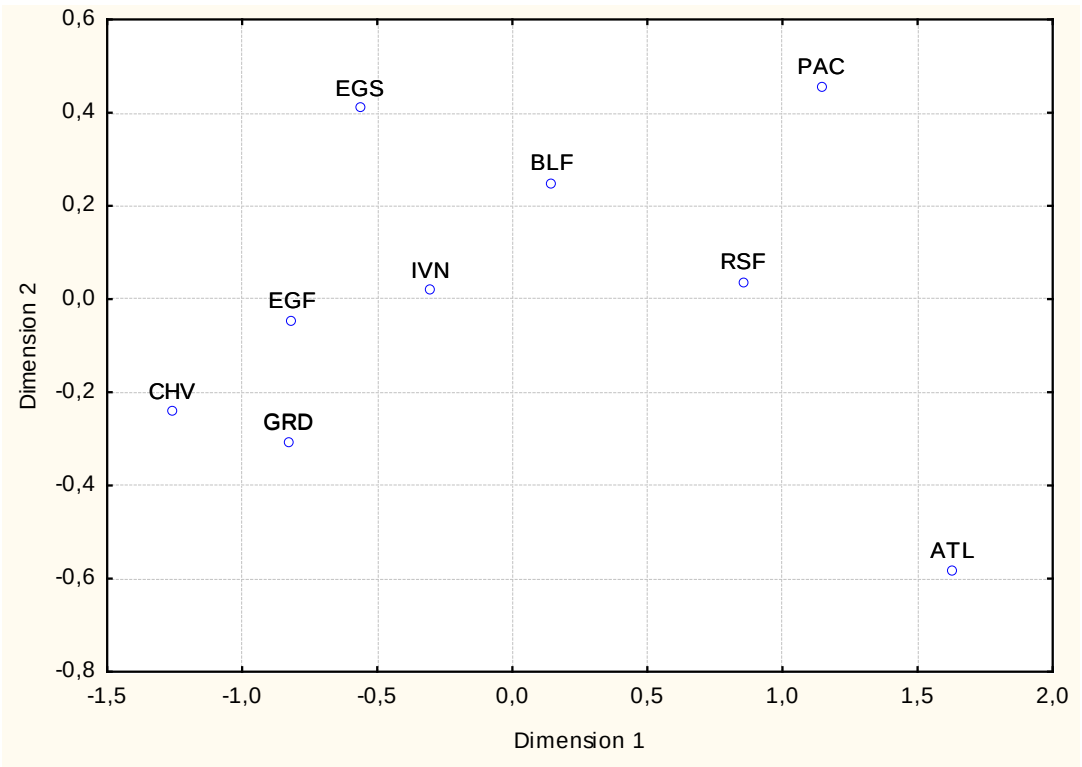

Рисунок 3.1.3. Результаты многомерного шкалирования выборок сельди для средних значений residuals, полученных на основе анализа 10 меристических признаков костей черепа. Обозначения выборок см. в табл.3.1.

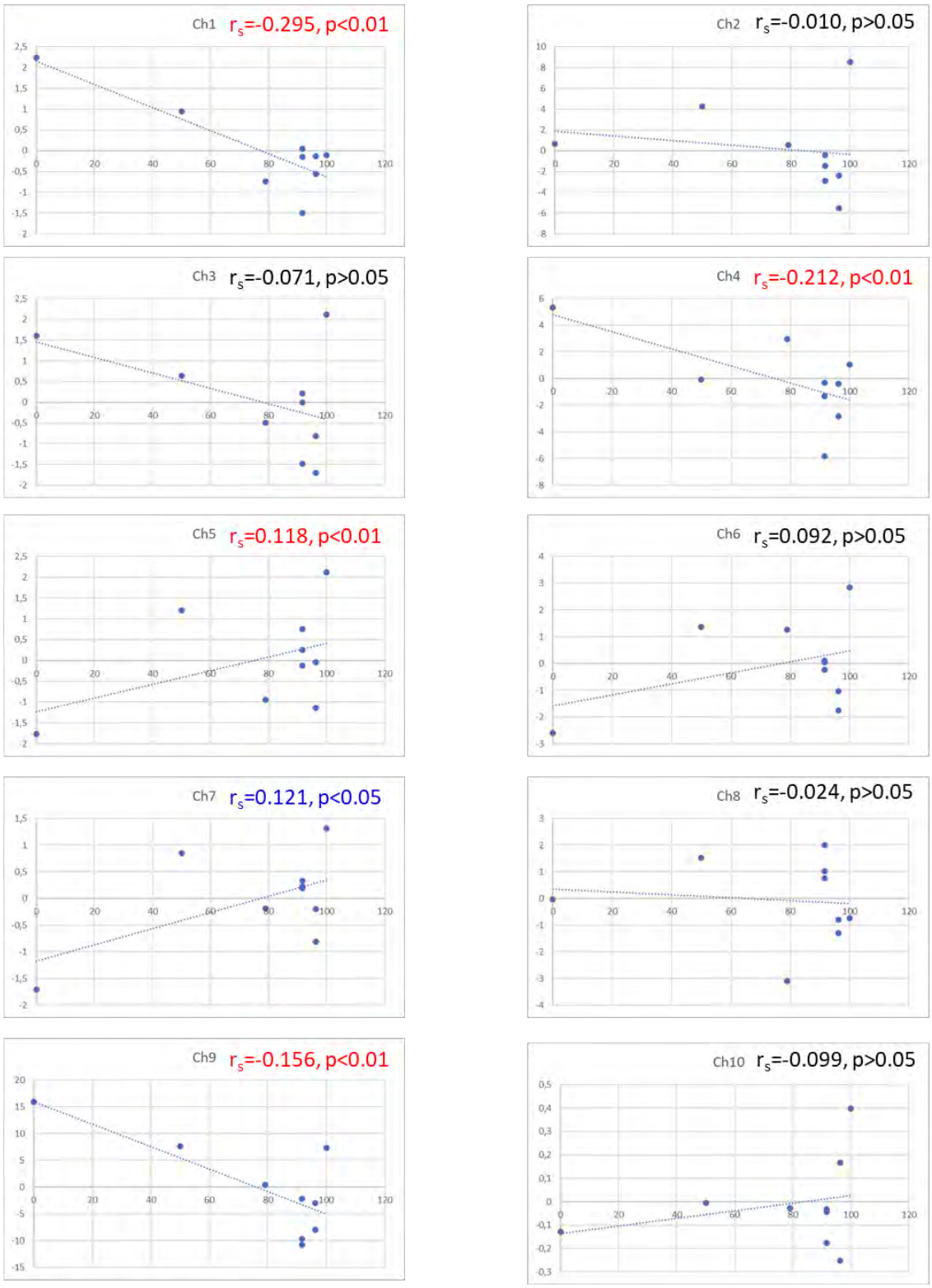

Рис. 3.1. 4. Связь между долей тихоокеанских генов в выборках и средним значением меристических признаков (residuals) для 10 изученных признаков (см. рис. 3.1.2). X-доля генов, Y – residuals. 296 особей, Spearman correlation

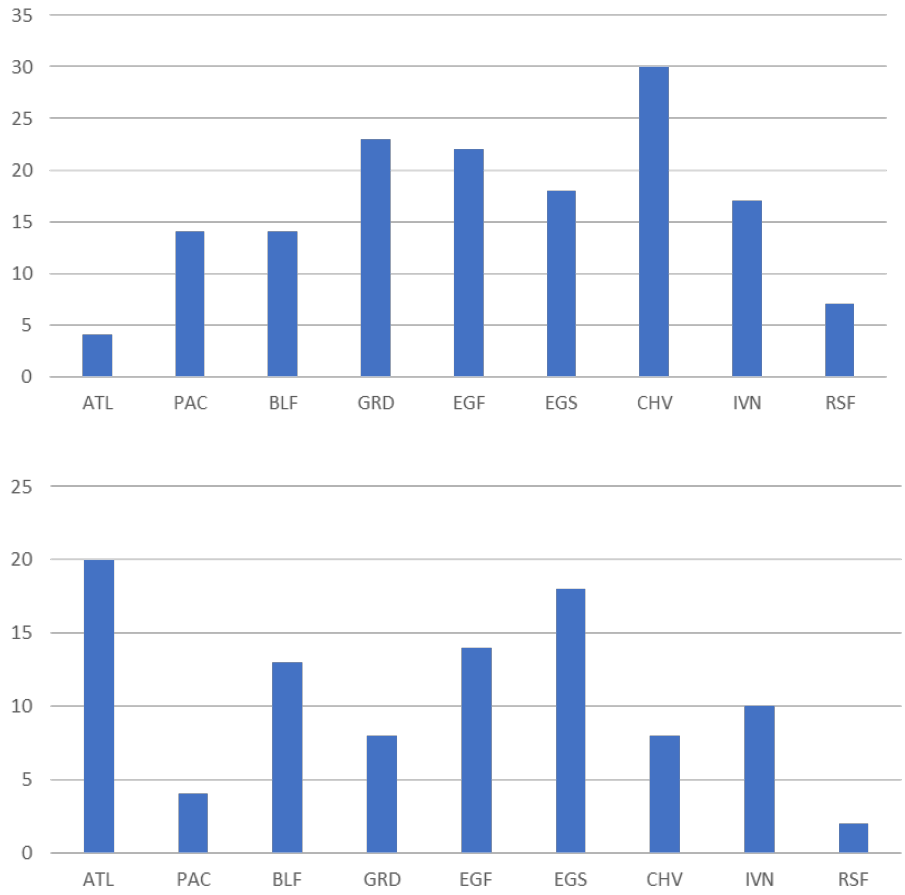

Рис. 3.1.5. Сумма рангов выборок по пористости костей. Вверху – кости articulare, dentale и parasphenoid (признаки 1, 4, 9), внизу – кости hyomandibulare и maxillare (признаки 5, 7).

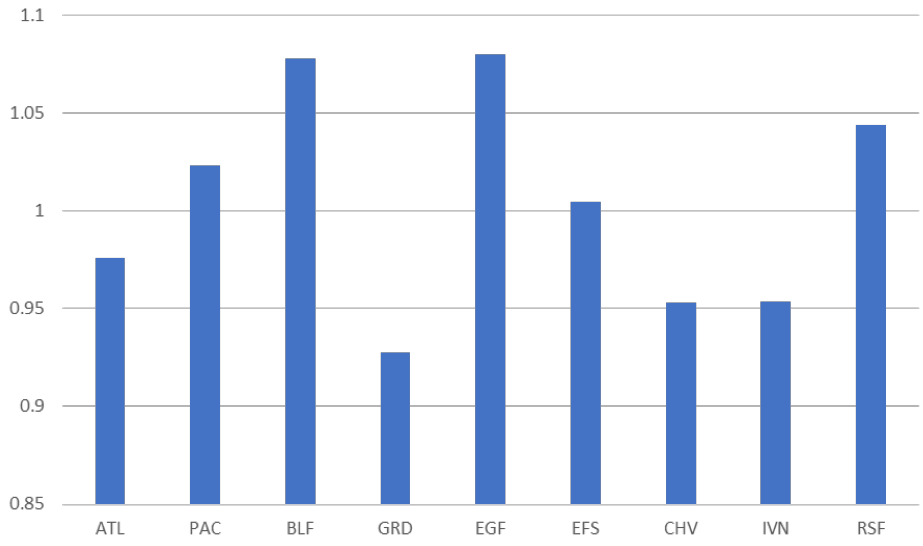

Рис. 3.1.6. Уровень флуктуирующей асимметрии разных выборок сельди. Для каждой выборки показан средний для 10 признаков уровень рангов индекса |L-R|/0,5*(L+R). Статистически достоверные попарные отличия (Mann-Whitney test, $p<0.05$) отмечены между выборками BLF и GRD, BLF и CHV, BLF и IVN, GRD и EGF, GRD и EGS, EGF и CHV, EGF и IVN.

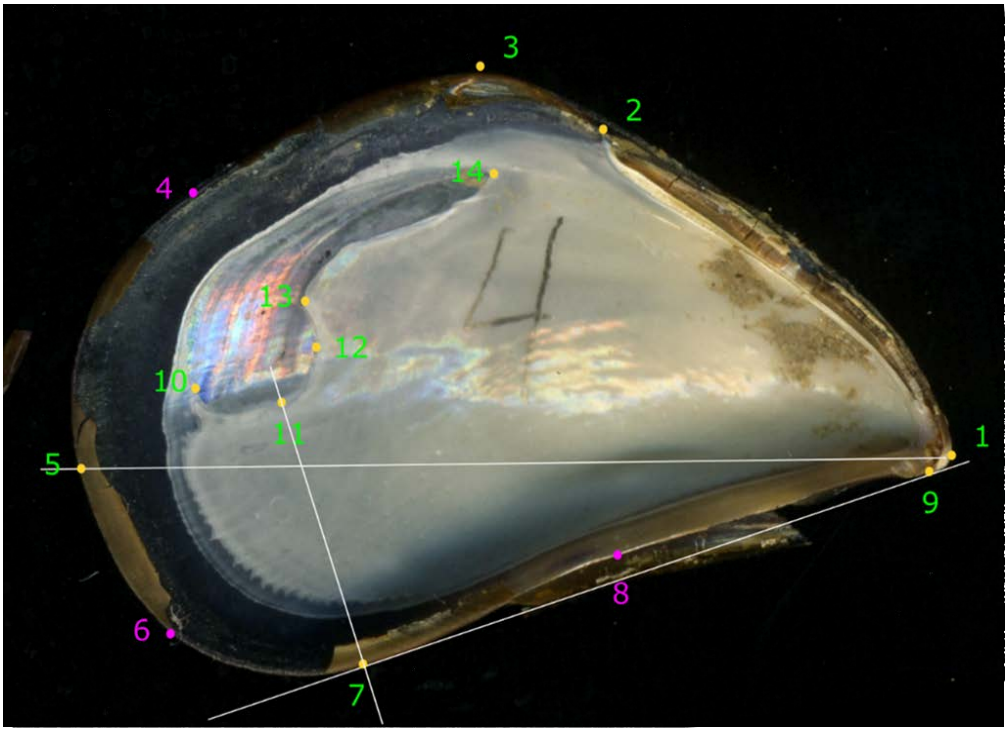

рис. 3.3.1. Расположение опорных точек, использованных для геометрической морфометрии раковин мидий

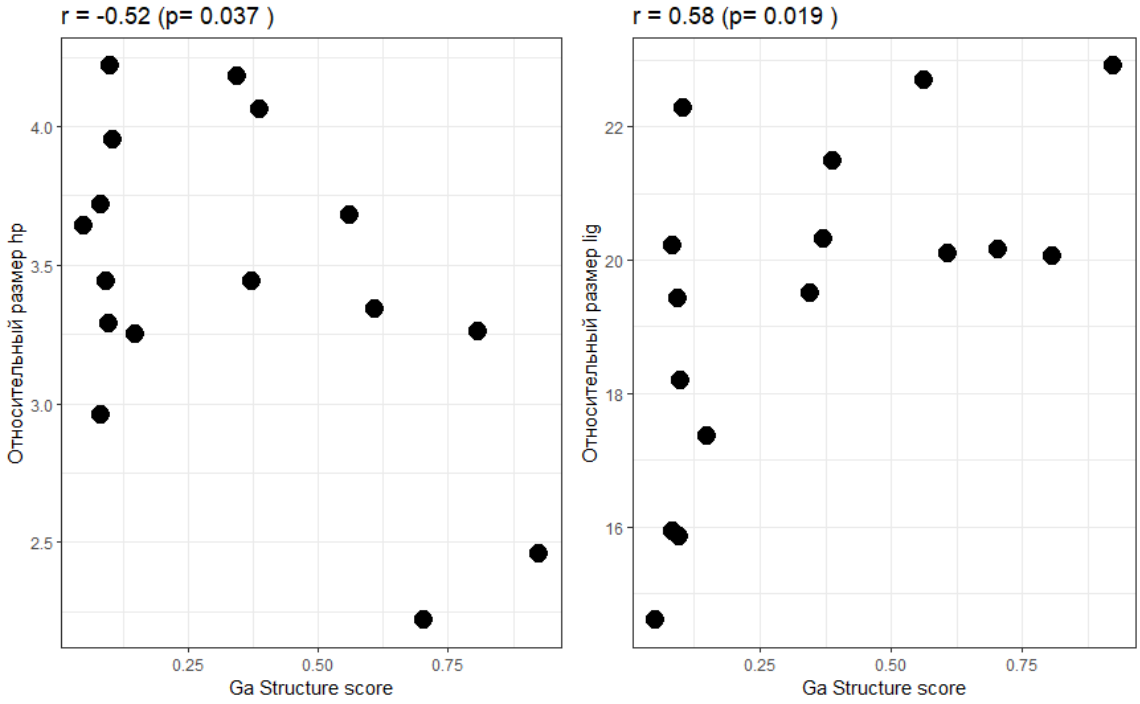

рис. 3.3.2. Связь «классических» морфометрических признаков раковин мидий из Гасейд с вероятностью присутствия в генотипе аллелей Ga. A. Относительный размер замковой площадки. B. Относительная длина лигамента. На графиках по OX – вклад генов M. galloprovincialis (индекс Structure). Приведены значения коэффициента корреляции и его статистическая значимость.

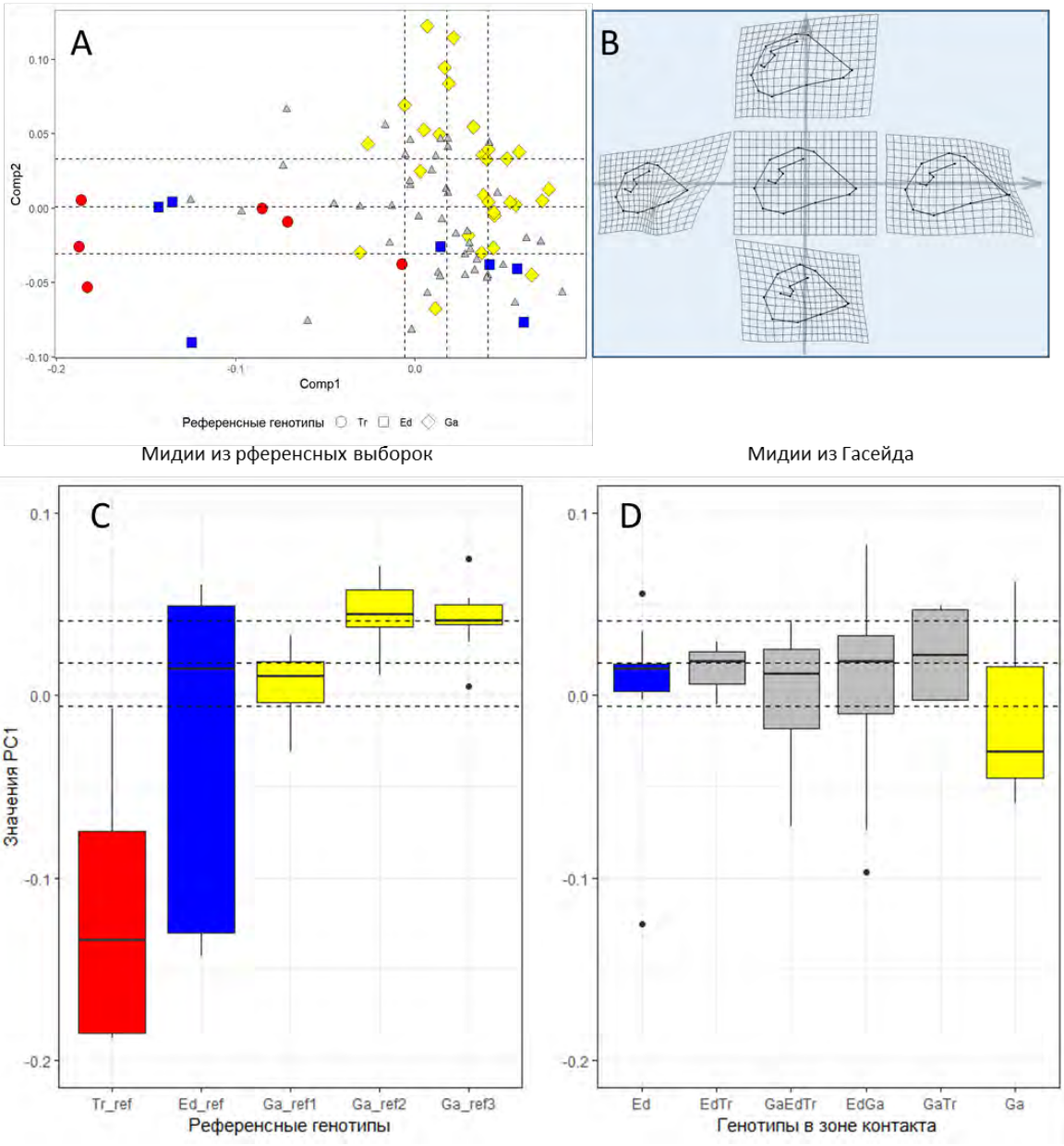

рис. 3.3.3. Вариация формы раковины мидий. A. Ординация мидий в морфопространстве первых двух главных компонент. Мидии из Гасейд показаны серыми треугольниками. Желтые, синие и красные точки – референсы M. galloprovincialis, M. edulis и M. trossulus, соответственно. Пунктирные линни отсекают границы квартилей каждой из компонент. B. Консенснусная форма раковины мидии (центральный рисунок) и формы, соответствующие минимальным и максимальным значениям двух главных компонент. C. Значения первой компоненты у моллюсков из референсных выборок. Цветовая кодировка как на графике A. D. Значения первой компоненты у моллюсков из Гасейд, классифицированных на категории: Ed – M. edulis, EdTr – гибриды M. galloprovincialis и M. edulis, GaEdTr – гибриды M. galloprovincialis, M. trossulus и M. edulis, GaTr – гибриды M. galloprovincialis и M. trossulus, Ga – M. galloprovincialis. На C и D прерывистые горизонтальные линии отсекают границы квартилей PC1.

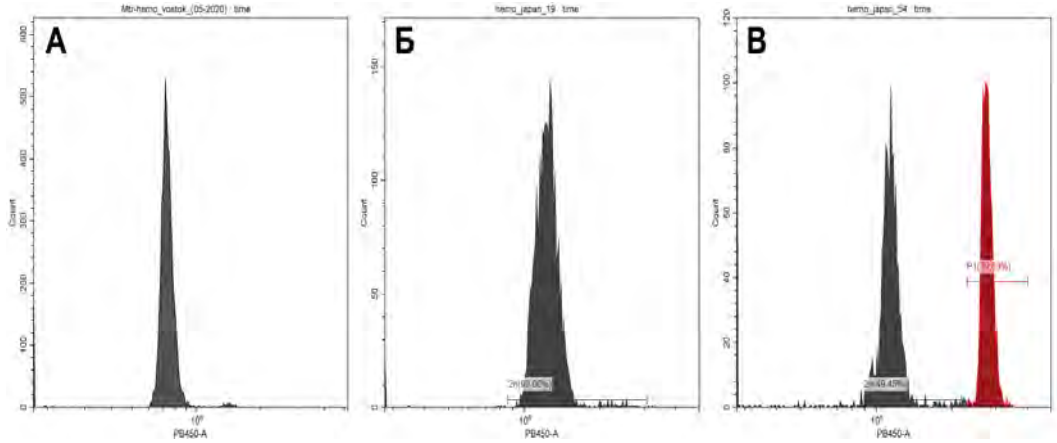

Рис. 4.1.1. Гистограммы распределения содержания ДНК в культивируемых гемоцитах мидии Mytilus trossulus. А – контрольные нормальные гемоциты 2020 года сбора; Б – нормальные гемоциты 2019 года сбора (проба № 19); В – аномальные гемоциты 2019 года сбора (проба № 54), красный пик – анеуплоидная субпопуляция клеток. По оси абсцисс – интенсивность флуоресценции DAPI, по оси ординат – количество событий.

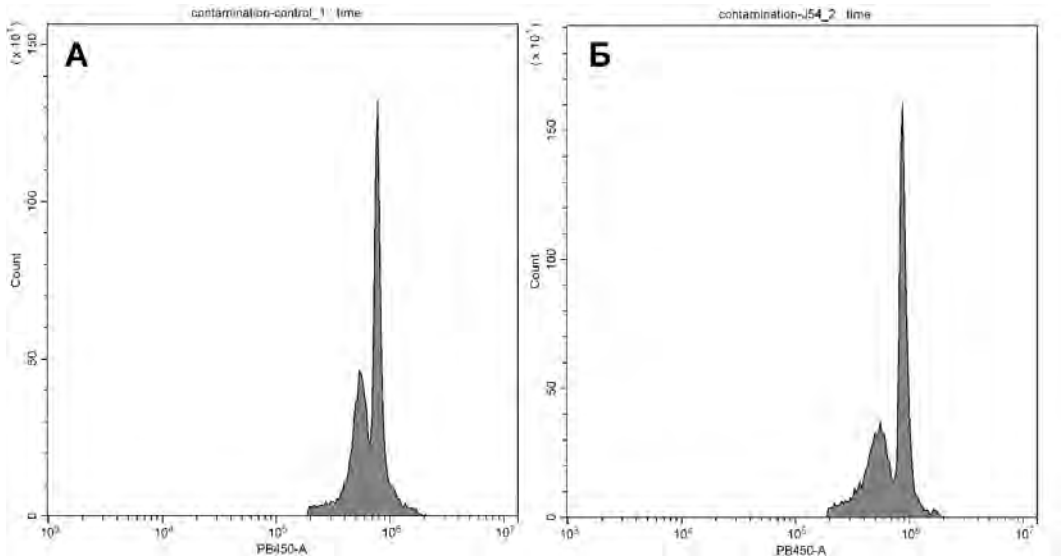

Рис. 4.1.2. Гистограммы распределения содержания ДНК в культивируемых гемоцитах мидии Mytilus trossulus. А – контрольные гемоциты 2020 года сбора после добавления нормальных гемоцитов 2019 года сбора (проба № 19); Б – контрольные гемоциты года сбора после добавления аномальных гемоцитов мидии 2019 года (проба № 54). По оси абсцисс – интенсивность флуоресценции DAPI, по оси ординат – количество событий.

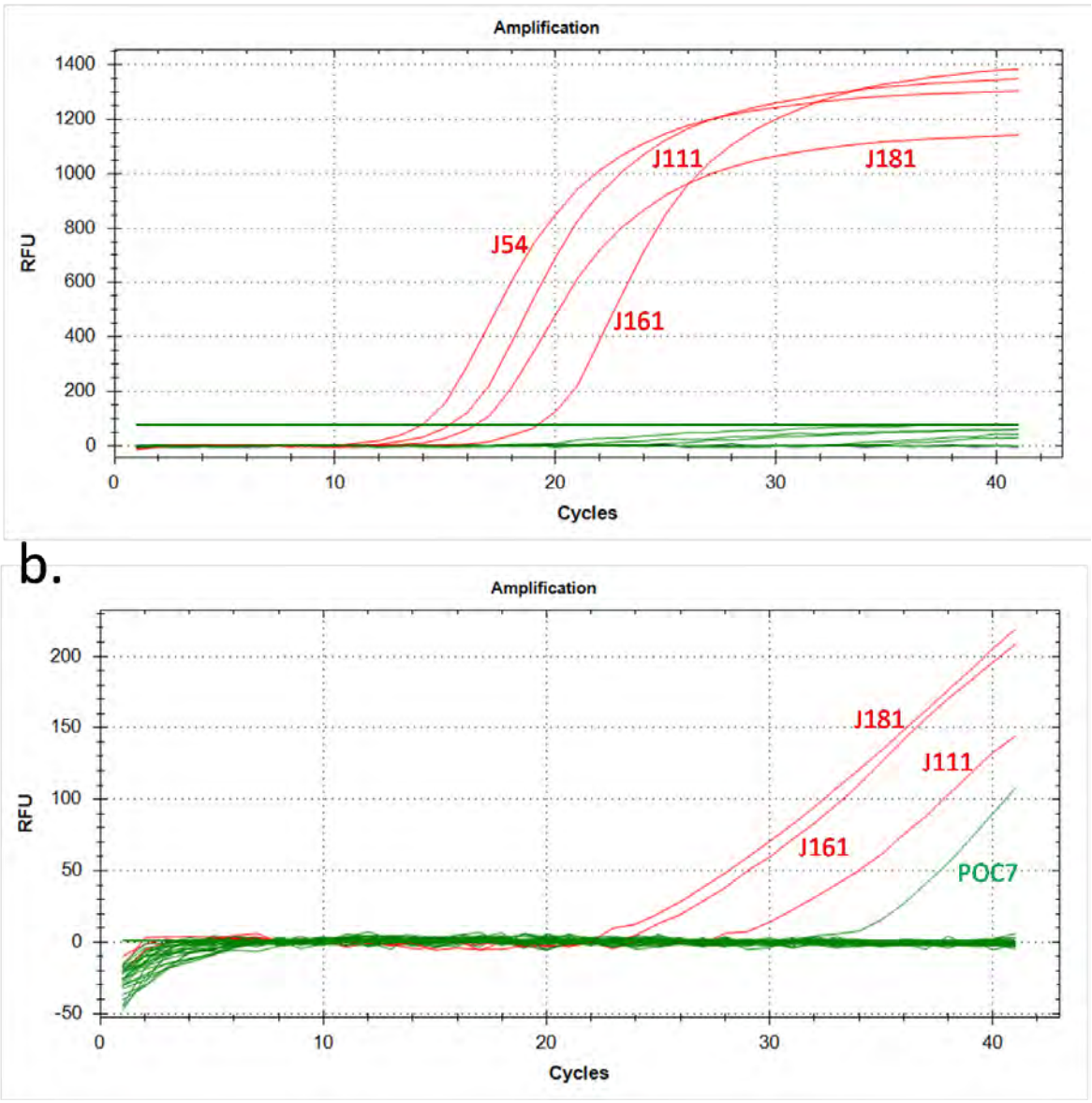

Рис. 4.2. Результаты ПЦР-РВ к аллелям EFalpha. По ОХ – число циклов реакции, по ОУ - уровень флюоресценции. a. Отработка условий ПЦР-РВ. Красные соответствуют положительным контролям (ДНК особей больных BTN2), зеленым – отрицательным контролям (ДНК здоровых особей). Амплификация детектируется только в положительных контролях. b. Применение метода на новом материале. В качестве положительных контролей использовано три образца. Отмечена амплификация продукта в одном из тестируемых образцов (POC7).

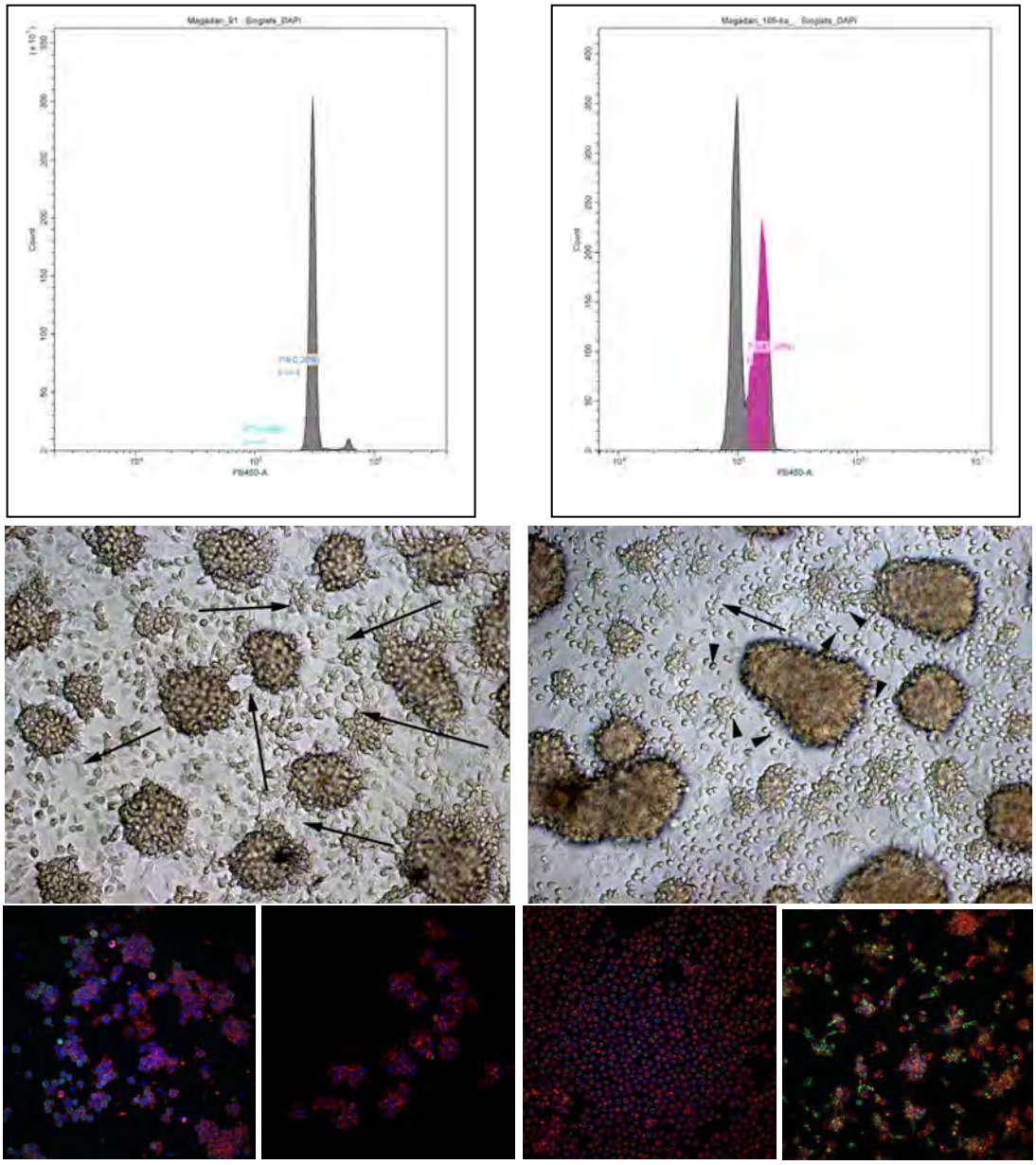

Рис. 4.3. Диагностика диссеминированной неоплазии у мидий Mytilus trossulus из Охотского моря. Верхний ряд: Цитометрический анализ гемолимфы здоровой (слева) и больной (справа) мидий. У больной мидии, помимо нормальных диплоидных клеток (серый пик), есть второй пик флюоресценции, соответствующий анеуплоидным клеткам (фиолетовый пик). По оси OX - уровень флюоресценции DAPI, по оси OY - событий. Средний ряд: общий вид гемоцитов здоровой (слева) и больной (справа) мидий под инвертированным микроскопом (объектив x20, Olympus CKX 41). В гемолимфе больной мидии, помимо нормальных распластанных гемоцитов, наблюдаются аномальные (круглые, плохо прикрепленные) гемоциты. Стрелки указывают на нормальные гемоциты, «головки» на аномальные гемоциты. Нижний ряд: иммунохимическая окраска гемоцитов разных больных (три левых фото) и одной здоровой (правая) мидии. Окраска на актин - красная; окраска антителами на тубулин – зеленая. Ядра окрашены DAPI (синяя окраска). Все аномальные гемоциты имеют увеличенное (как правило, лопастное) ядро и необычный цитоскелет (гемоциты, в основном, круглые, в отличие от контрольных распластанных). Препараты анализировали на конфокальном лазерном микроскопе Zeiss LSM 780. Объектив x40 кроме левого фото (x65).

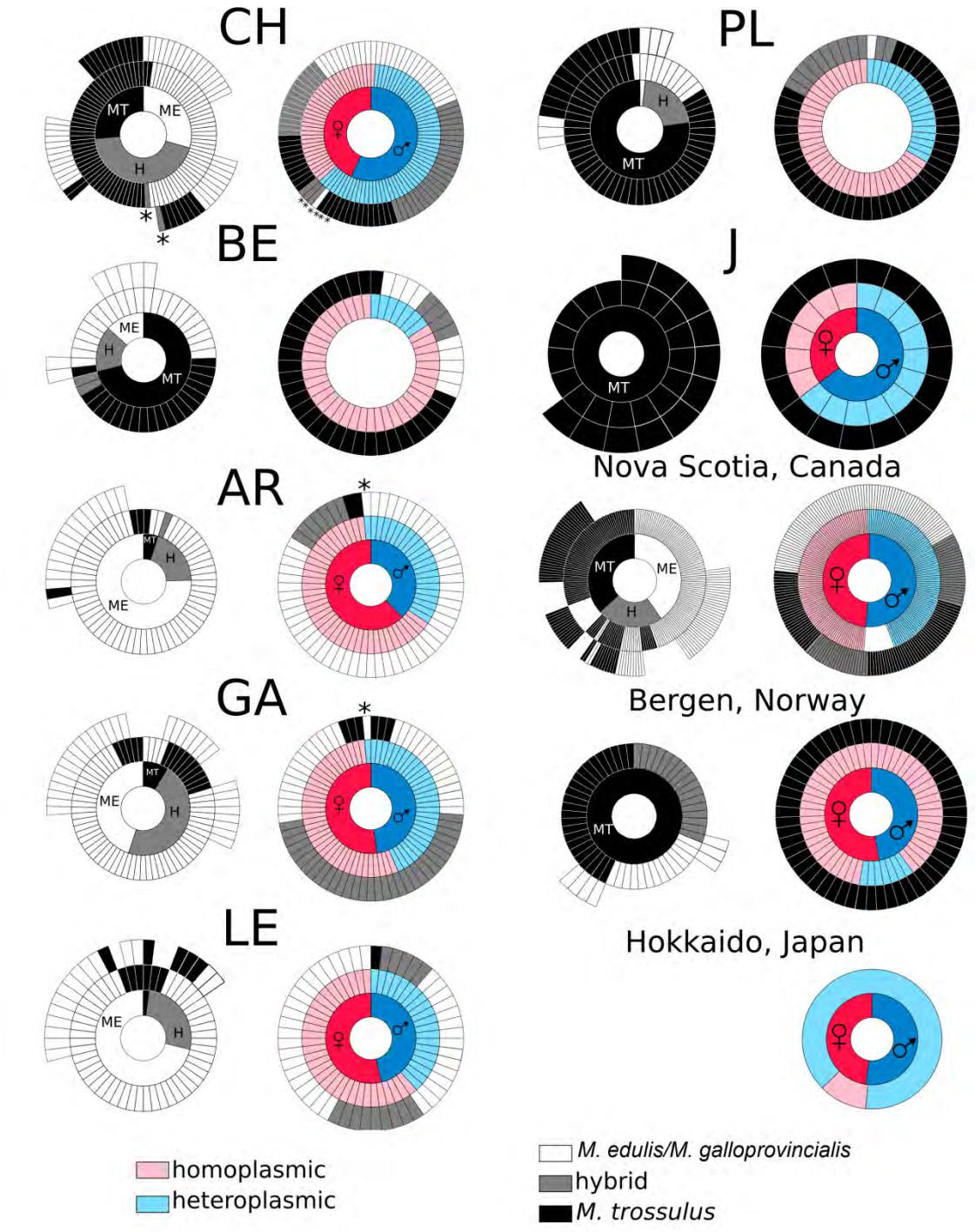

Рис. 4.4.1. Анализ согласия между физиологическим и «митохондриальным» полом, и между видовым ядерным и мтДНК генотипами у мидий Mytilus spp. Выборки: CH – Белое море, J – Японское море, BE, AR, GA – Норвегия, LE, PL – Шотландия (наши данные), Nova Scotia, Канада (Saavedra et al, 1996), Bergen, Норвегия (Smietanka & Burzynski, 2017), Hokkaido, Япония (Brannock et al, 2013). На диаграммах сектор – особь. На левых диаграммах результаты мтДНК генотипирования особей соотнесены с их видопринадлежностью по ядерным локусам: внутренний круг отражает вид или гибридный статус особей по мультилокусным ядерным данным (M. edulis, M. trossulus или гибриды), средний круг – видопринадлежность F-мтДНК особей, внешний круг - наличие/отсутствие M-мтДНК и ее видовую принадлежность. На правых диаграммах результаты мтДНК генотипирования особей соотнесены с их физиологическим полом: внутренний круг показывает физиологический пол, средний круг – «митохондриальный пол», внешний круг – видовой статус особи по ядерным локусам. Звездочками отмечены нарушения DOI.

a.

	D alleles, p-value	C alleles, p-value
RDP	-	-
GENECONV	$4.668*10^{-5}$	-
Bootscan	$5.704*10^{-3}$	-
Maxchi	$1.556*10^{-9}$	$4.229*10^{-2}$
Chimaera	$1.145*10^{-4}$	-
SiScan	$6.138*10^{-11}$	$1.248*10^{-17}$
3Seq	$1.042*10^{-14}$	$9.983*10^{-6}$

b.

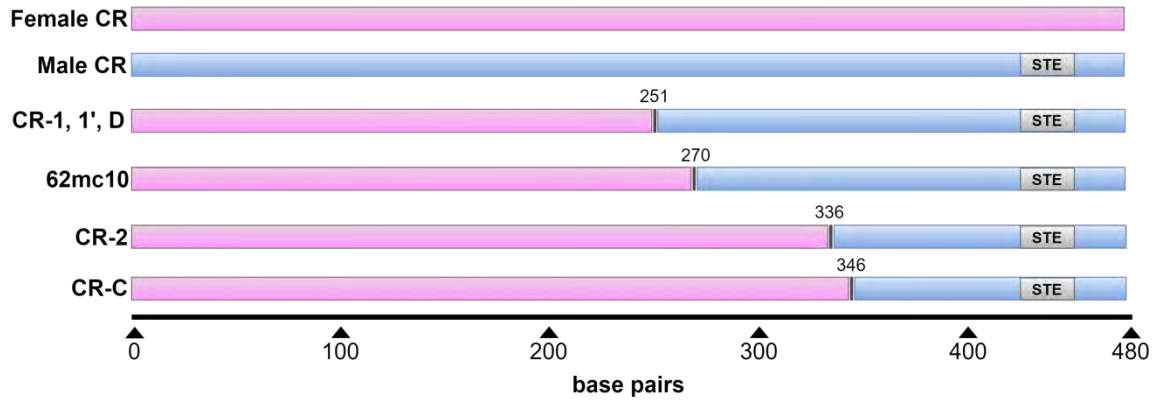

Рисунок 4.2.2. Анализ фрагмента 16S-CR 620 п.н. BTN2 мидий M. trossulus из Приморья на предмет точек рекомбинации между F-мтДНК и M-мтДНК. **a**. Приведены результаты анализа (p-value) выравнивания в программе RDP4. Для выравнивания использованы фрагменты контрольных регионов мтДНК СТС мидий из Приморья (наши данные, гаплотипы CR-1, 1', 2), из Чили (Yonemitsu et al, 2019, CR-C, D), предположительно раковый геном из Балтики (Smietanka & Burzynski, 2017, 62mc10) и референсные контрольные регионы F-мтДНК и M-мтДНК M. trossulus из NCBI. Алгоритмы, реализованные в программе RDP4 детектируют события рекомбинации в 62mc10, в гаплотипах «группы C» (CR-C, 2) и «группы D» (CR-1, 1’, D). **b.** Схема выравнивания использованного для поиска точек рекомбинации. Прямоугольники соответствуют нуклеотидной последовательности. Розовым цветом обозначена F-мтДНК, голубым M-мтДНК. Обнаруженные методом рекомбинации отмечены черными вертикальными линиями, номер возле них указывает на нуклеотидную позицию от начала выравнивания. RDP4 обнаружила точку рекомбинации в одной и той же нуклеотидной позиции в гаплотипах группы D; точки рекомбинации в гаплотипах CR-2 и CR-C оказались близкими, но не идентичными. Точка рекомбинации в аллели 62mc10 ближе к таковой у аллелей группы D. Последовательность ответственная за наследование мтДНК по мужской линии отмечена серым блоком «STE» (от «sperm transmissible element»).

Submissions Being Processed for Author Vadim Mikhailovitch Khaitov, Ph.D.

Page: 1 of 1 (1 total submissions) Display 10 results per page.

Action	Manuscript Number	Title	Initial Date Submitted	Current Status
View Submission Send E-mail	PONE-D-20-30389	Species identification based on a semi-diagnostic marker: evaluation of a simple conchological test for distinguishing blue mussels Mytilus edulis L. and M. trossulus Gould	Sep 26 2020 4:41PM	Under Review

Page: 1 of 1 (1 total submissions) Display 10 results per page.

<< Author Main Menu

Possible titles:

First description of a widespread *Mytilus trossulus*-derived bivalve transmissible cancer lineage in *M. trossulus*

The Russian trail in blue mussel transmissible cancer: first description of a widespread *Mytilus trossulus*-derived cancer lineage in *M. trossulus*.

Searching for the birthplace of blue mussel transmissible cancer: first description of a widespread *Mytilus trossulus*-derived cancer lineage in *M. trossulus*.

The root of the transmissible cancer: first description of a widespread *Mytilus trossulus*-derived cancer lineage in *M. trossulus*.

Skazina M., Ivanova A., Maiorova M., Vainola R., Odintsova N, Strelkov P.

Abstract

Two lineages of bivalve transmissible neoplasia (BTN), BTN1 and BTN2, are known in blue mussels *Mytilus*. Both lineages derive from the Pacific mussel *M. trossulus* and are identified primarily by the unique genotypes of the nuclear gene EF1α. BTN1 is found in populations of *M. trossulus* from the Northeast Pacific, while BTN2 has been detected in populations of other *Mytilus* species worldwide but not in *M. trossulus* itself. The aim of our study was to examine mussels *M. trossulus* from the Sea of Japan (Northwest Pacific) for the presence of BTN. Using hemocytology and flow cytometry of the hemolymph, we confirmed disseminated neoplasia in our specimens. Cancerous mussels possessed the unique BTN2 EF1α genotype and two mitochondrial haplotypes with different recombinant control regions, similar to that of common BTN2 lineages. This is the first report of BTN2 in its original host species *M. trossulus*. *M. trossulus* populations in West Pacific may be the birthplace of BTN2 and a natural reservoir where it is maintained and whence it spreads worldwide. A comparison of all available BTN and *M. trossulus* COI sequences suggests a common and recent, though presumably prehistoric origin of BTN2 diversity in populations of *M. trossulus* outside the Northeast Pacific.

Introduction

Clonally transmissible cancer (CTC) is a neoplastic disease passed from individual to individual by physical transfer of cancer cells[1–3]. The first inkling of a transmissible cancer came from a study of canine transmissible venereal sarcoma, CTVT[4], dating back to 1876. Since then CTC has been confirmed for CTVT[5] and the facial tumor of Tasmanian devil *Sarcophilus harrisii*[6,7] and, more recently, for several lineages of disseminated neoplasia (DN) of six marine bivalve mollusks: *Mya arenaria*[8], *Cerastoderma edule*, *Mytilus trossulus*, *Polititapes aureus*[2], *Mytilus edulis*[9] and *Mytilus chilensis*[10].

A straightforward method of CTC diagnostics is DNA genotyping. In case of CTC, the genotype of cancer cells is different from that of the host cells. The result is genetic chimerism, when an individual possesses cells with different genotypes[9]. At the same time, cancer cells of the same lineage have the same genotype in different infected individuals. Such lineage-specific genotypes are thought to derive from the ~~–~~patient zero", the host individual in which the cancer originated[2,8,11,12].

The finding that CTC is behind DN in six bivalve species is fairly recent, which suggests that more such discoveries are in store. Some indirect evidence also points to a widespread occurrence of transmissible cancers in bivalves[13]. At the same time, there are not enough data to be sure whether CTC is the only cause of DN in those six species or whether it is the usual cause of DN in bivalves in general.

DN is a fatal leukemia-like cancer affecting many marine bivalves[14]. It was first described in *M. trossulus* from the Northeast Pacific almost half a century ago[15]. DN is manifested in an uncontrolled proliferation of neoplastic cells in the hemolymph[16], which ultimately replace healthy hemocytes. To note, though neoplastic cells are usually also referred to as hemocytes, their tissue origin remains unknown[14,17].

Normal hemocytes of healthy bivalves (agranulocytes and granulocytes) are diploid and have a low mitotic activity[18,19]. Neoplastic hemocytes are aneuploid[18–22], and have a high proliferation rate and a striking morphology. They are rounded, with a high nucleus-to-cytoplasm ratio[14,22,23], and their nucleus is pleomorphic (i.e. variable in shape), 2-4 times larger than that of normal hemocytes. As the disease progresses, the proliferating cells infiltrate other tissues, which leads to the loss of integration and normal functioning of organs[24,25]. DN may reach epizootic level, causing mass mortality in wild and commercial bivalve populations[14,22,24].

There are two approaches to DN diagnostics. The first approach is based on direct examination of cells in hemolymph smears or tissue sections. Various hemocytological techniques may be

employed such as light microscopy of fresh or stained hemolymph smears, confocal microscopy of hemocytes stained with fluorescent dyes or with monoclonal antibodies specific to neoplastic cells, and immunochemistry with antibodies specific to mitotic spindles (for revealing proliferating cells). The second approach is based on measuring DNA content. It may employ flow cytometry of hemocytes labeled with fluorescent dyes specifically binding DNA or karyotypic analysis[25,26]. Flow cytometry is less sensitive to the initial stages of DN than hemocytology but allows a time-efficient examination of large samples[19,22].

Smooth-shelled blue mussels of the *Mytilus edulis* species complex are widely distributed in cold-temperate seas of the Northern (*M. edulis*, *M. trossulus*, *M. galloprovincialis*) and the Southern (*M. galloprovincialis*, *M. chilensis*, *M. platensis* and *M. planulatus*) Hemisphere[27,28]. They have been reported to harbor two presumably independent CTC lineages, BTN1 and BTN2 (Yonemitsu et al., 2019). Both lineages derived from *M. trossulus*, i.e. they have its genome. They are marked by different alleles of mitochondrial and nuclear loci, the best diagnostic marker for both lineages being the gene coding the elongation factor one alpha (EF1α)[2,10]. BTN1 was described in populations of its original host species in British Columbia (Northeast Pacific). BTN2 has been found in *M. edulis* from Western Europe (Northeast Atlantic), in *M. chilensis* from Southern Chile (Southeast Pacific) and from Beagle Channel in Argentine (Southwest Atlantic), but not in *M. trossulus* itself[2,10]. Yonemitsu et al., 2019 suggested that the original host, *M. trossulus*, could have evolve resistance to BTN2. Mitochondrial genomes BTN2 clones from *M. chilensis* in Chile have been reported to be the product of recombination between the cancer (i.e. *M. trossulus*-derived) and the host (*M. chilensis*) mitogenome[10].

So, *M. trossulus* gave rise to at least two CTCs, BTN1 and BTN2. BTN2 is a cross-species cancer, which is supposedly prone to occasional mitochondrial capture from the transient host and subsequent mitochondrial DNA recombination between the cancer and the host. Taken individually, these features are not unique. Two independent lineages of the facial tumor affecting Tasmanian devils are known[29]. Neoplastic hemocytes in the bivalve *P. aureus* have the genotype of another bivalve, *Venerupis corrugata*, for which CTC has not been reported[2]. Multiple episodes of mitochondrial capture from hosts and recombination between cancer and host mitogenomes are confirmed for CTVT[30].

The geographical distribution of BTN is understudied, also in its original host species. *M. trossulus* is basically a North Pacific species, which has spread to many areas of the North Atlantic in a series of repeated invasions[31,32]. In the Pacific it is distributed from the Arctic to the Bay of California along the American coast and to the Sea of Japan along the Asian coast[27]. Only American Pacific populations of *M. trossulus* have been screened for BTN[2]. Riquet et al. (2017)

and Yonemitsu et al. (2019) compared BTN mitochondrial sequences with all publically available *M. trossulus* sequences. Considering the common properties of mitochondrial sequences derived from BTN2, an individual 62mc10 of *M. trossulus* from the Baltic (NCBI accession number KM192133[33]) and individuals from Norway[34], Yonemitsu et al (2019) hypothesized that BTN2 lineage originated in a North European *M. trossulus* population. DN has indeed been recorded in *M. trossulus* in the Baltic Sea[35]. However, it was also found in the Sea of Japan[36], one of the two macroregions within the ancestral range of *M. trossulus*. We know that populations on the American East Pacific coast are infected with BTN1, but what about those on the opposite side of the Ocean?

The aim of our study was to examine the populations of *M. trossulus* from the Sea of Japan for the presence of BTN and, should it be found, to establish its genetic affinity with the known BTN lineages.

Material and methods

Study design

The workflow of the study is schematically depicted in Figure 1. In brief, mussels were collected in the Gulf of Peter the Great, the Sea of Japan. Different tissues were sampled from each individual (*"Sample collection and preprocessing"* step). The hemolymph of all mussels was analyzed by flow cytometry. Based on the results, the mussels were preliminary classified as cancerous (DN-suggested) if an increased fraction of aneuploid hemocytes was registered. For five mussels (four DN-suggested and a control healthy one) the diagnosis was verified by direct examination of hemocytes using hemocytology and immunochemistry (*"DN diagnostics*"). The same cancerous mussels plus control ones were used during the next steps. There, we generally followed the methodology from the pioneer researches of BTN[2,9,10]. Hemolymph and foot tissues were genotyped separately for nuclear microsatellites and EF1α and for mitochondrial cytochrome oxidase subunit I (COI) and control region (CR). For EF1α and CR, when multiple alleles were present and could not be resolved by sequencing, molecular cloning was employed. Two things were considered as an evidence of BTN: genetic chimerism of cancerous individuals, with the hemolymph and the foot tissues being dominated by different sets of alleles, and the identity of "extra" alleles of different cancerous individuals (see Introduction) (*"BTN diagnostics*"). At the step of *"Phylogenetic analyses*", evolutionary relationships of cancer-associated genotypes were revealed. In one analysis all corresponding BTN sequences from the previous studies were considered in order to identify the known cancer lineages, if any, affecting mussels from the Sea of Japan. In another analysis, all available *M. trossulus* COI sequences

were examined in order to find out whether the cancer alleles identified in the Sea of Japan mussels had been recorded anywhere before and whether they demonstrate an affinity to particular mitochondrial lineages of the host. Finally, we verified the purebred *M. trossulus* ancestry of mussels from BTN-infected population by genotyping them by three additional taxonomically diagnostic markers (“*Species confirmation*”) and identified their sex histologically and/or genetically (“*Sex identification*”).

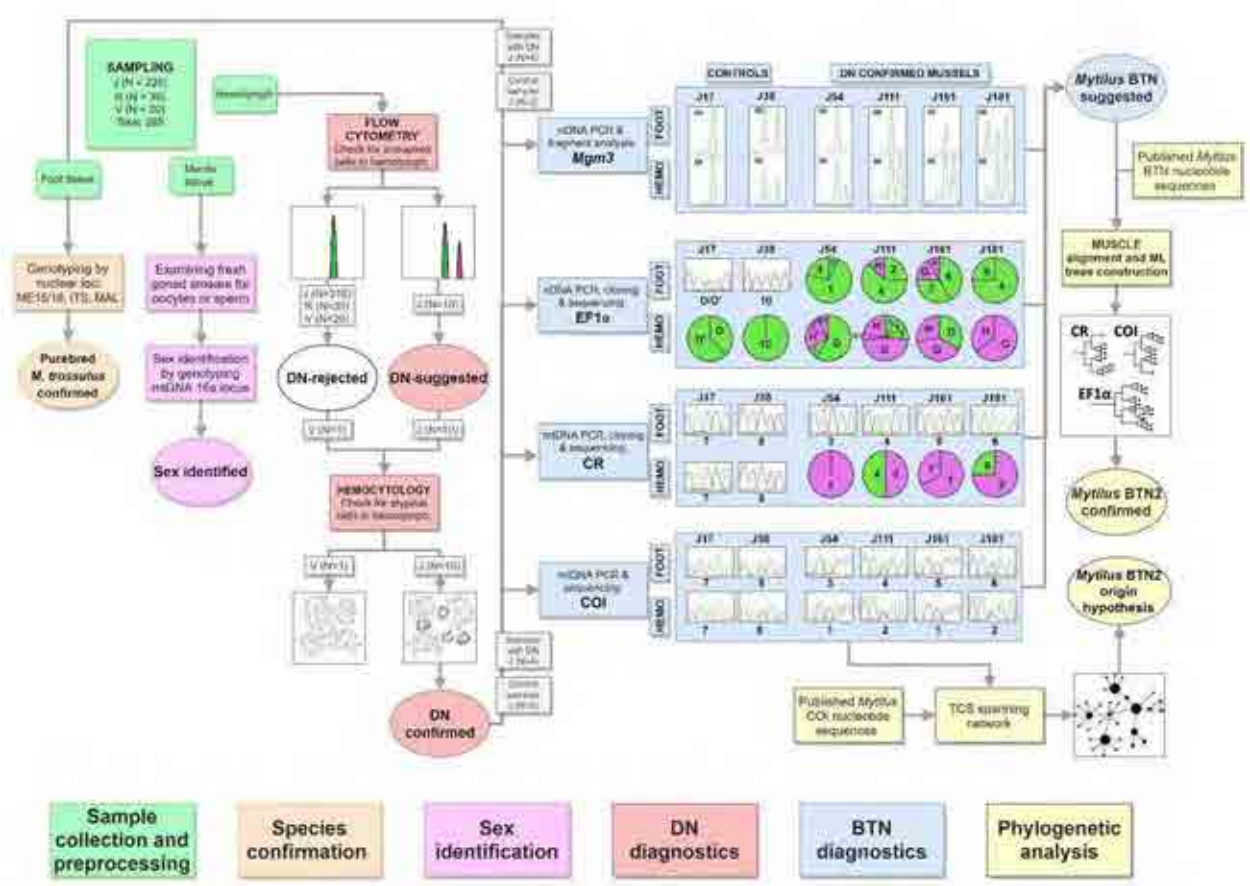

Figure 1. Study design. Different steps of work are color-coded (see boxes at the bottom). Unique numbers of mussels used at different steps are given. Main results of the analyses are schematically outlined (see text). Real microsatellite electropherograms are presented. Sectors of pie charts are frequencies of sequences revealed by molecular cloning. Sequences are indicated by their unique names; supposedly cancerous alleles are shown in purple.

Sample collection and preprocessing

Mussels were collected by scuba diving at three localities of the Sea of Japan in July-September 2019: Vladivostok city public beach “Vtoraya Rechka” (43°10'02"N, 131°58'07"E, depth 5 m, a natural bottom habitat, sample size N=39, mean shell size L=25 mm, sample “R”), “Vostok” Marine Biological Station (42°89'3528"N, 132°73'3271"E, depth 5 m, experimental mussel plantation, N=20, L=50 mm, sample “V”) and the Gaydamak Bay (42°52'04.2"N, 132°41'27.2"E, fouling of a mooring buoy anchored at a depth about 5 m about 50 m from the shore, N=226, L=37 mm, sample “J”). “Vostok” station is a nature reserve and the least polluted of the studied localities, while Gaydamak is an industrial harbor heavily polluted by sewage.

After sampling, the mussels were transported to the laboratory and stored for 2-4 days alive, each sample in a separate aquarium, before the experiments.

Hemolymph was collected from the posterior adductor with the help of a syringe with a 22-gauge needle. Some aliquots of hemolymph were used immediately for flow cytometry, and some were fixed in 4% PFA for future immunochemistry studies. Some aliquots, as well as pieces of mantle and foot tissues from each specimen, were fixed in 70% ethanol for genetic analyses.

DN diagnostics

Flow cytometry

100 µl of fresh hemolymph from each mussel were incubated in cold 70% ethanol for 40 min. Ethanol was removed by centrifugation and the cells were washed twice with phosphate buffer saline (PBS, Sigma). Finally, the cell pellet was resuspended in 100 µl of PBS with 5 µl of 100x 4'-6-diamidino-2-phenylindole (DAPI). DAPI-stained hemocytes were analyzed on a CytoFLEX flow cytometer with CytExpert software (Beckman-Coulter, USA). Flow cytometry analysis and the interpretation of the results followed Vassilenko & Baldwin (2014). Plots of side scatter SSC-A versus forward scatter FSC-A were used for visualization of cell groups. Duplets were removed by gating on forward scatter height FSC-H against forward scatter FSC-A. Histograms of fluorescence signal PB450-A were used for determination and gating of cells with different levels of ploidy. At least 10,000 events were evaluated for each sample. Histograms of PB450-A were used to estimate ploidy levels of aneuploid peaks relative to the diploid peak of the same specimen and the rate of aneuploid cells in the sample. Mussels were diagnosed as healthy (“~~D~~N-rejected”) if the scatter plot SSC-A *vs* FSC-A and PB450-A histogram of fluorescence indicated only non-proliferating cells (agranulocytes and granulocytes) with one peak for diploid phase or with admixture of very few (<5%) proliferating cells (minor peak for tetraploid cells). If a cell population with additional peaks was detected, the individuals were considered as “~~D~~N-suggested”.

Hemocytology and immunochemistry

All procedures for cell fixation and staining were described in detail in a previous study[37]. In brief, the cells were stained with TRITC-labeled phalloidin (Molecular Probes) and DAPI (Vector Laboratories) for visualization of actin cytoskeleton and nucleus. We used primary mouse monoclonal antibodies against anti-α-acetylated tubulin (clone 6-11B-1, Sigma Aldrich and proliferating cell nuclear antigen (PCNA, clone PC10, Abcam) for detecting mitotic spindles and proliferating cells, respectively. These antibodies were previously characterized as labeling

dividing cells in bivalves[37–40]. Observations and images were made with Zeiss LSM 780 confocal laser scanning microscope. A mussel was considered as ~~–~~DN-confirmed" if non-adherent hemocytes with a high nucleus-to-cytoplasm ratio and a pleomorphic nucleus were detected.

BTN diagnostics

Total DNA was extracted separately from the hemolymph and the foot tissue~~s~~ using the DNeasy Blood and Tissue Kit (Qiagen, USA) according to the manufacturer's protocol.

The microsatellite markers *Mg*μ3, *Mg*μ5, *Mg*μ6, *Mg*μ7 polymorphic for *M. trossulus* were amplified according to the protocol in the original study[41] and subjected to fragment analysis by capillary electrophoresis. Microsatellite fragment patterns were analyzed in GelQuest (https://www.sequentix.de/gelquest/help/index.html).

Three DNA fragments—an intron-spanning region of EF1α gene, a fragment of COI and a fragment spanning 16S rRNA and CR—were amplified using primer sequences and PCR cycling conditions as in Metzger et al. (2016) and Yonemitsu et al. (2019) and sequenced in both directions by Sanger method. To specify, the primers used for COI amplification target female mitochondrial genome (F-mtDNA), while primers for 16s and CR region potentially amplify both male (M-mtDNA) and F-mtDNA[10]. Due to the doubly uniparental inheritance (DUI) blue mussel females are homoplasmic for F-mtDNA, which is inherited maternally, while males are heteroplasmic, carrying the F-mtDNA in somatic tissues and the paternally inherited M-mtDNA in gonads[42].

Sequencing and fragment analysis were performed on Genetic Analyzer ABI Prism 3500xl at the Centre for Molecular and Cell Technologies of St. Petersburg State University Research Park (https://researchpark.spbu.ru/en/biomed-eng). Sequence chromatograms were visually studied in MEGA X software[43].

EF1α PCR products from the hemolymph and the foot tissues of the cancerous and the control mussels were subjected to molecular cloning. CR PCR products were cloned from the hemolymph of the cancerous mussels only. Molecular cloning procedures were subcontracted to Evrogen JSC (Russia). Quick-TA kit (Evrogen JSC) was used for cloning, and the plasmids were transformed into competent *E. coli* (Evrogen JSC). In all the cases at least 16 colonies were sequenced using M13 primers. Some sequences were detected only in one colony. They were probably artificial mutations generated by PCR and molecular cloning procedures such as polymerase errors and random crossing-over of incomplete PCR extension products of original alleles[44,45] and therefore were excluded from the following analyses.

In COI, signals from multiple alleles were resolved by sequencing only. If "piggybacks", that is, overlapping peaks at some positions, were observed on chromatograms, the major peaks were attributed to the presumably cancer allele in the hemolymph samples and to the presumably host allele in the foot samples. We never observed signals from more than two alleles on COI sequencing chromatograms (see Results).

Sequence chromatograms were analyzed in MEGA X[43]. Sequences were aligned with MUSCLE algorithm (https://www.ebi.ac.uk/Tools/msa/muscle/) with some manual adjustment.

Phylogenetic analysis

Nucleotide sequences of CR, COI and EF1α from four cancerous mussels were aligned together with the corresponding sequences from a previous BTN study (data on 11 mussels with confirmed BTN)[10] and mitochondrial sequences of the Baltic mussel 62mc10[33]. The 62mc10 genome was previously shown to be similar to cancerous ones[10]. Alignment was done by MUSCLE algorithm (https://www.ebi.ac.uk/Tools/msa/muscle/) with some manual adjustment. Maximum likelihood phylogenetic trees were generated using MEGA X[43], with 100 bootstrap replicates, treating gaps in the alignment as missing data. The same substitution models as in Yonemitsu et al (2019) were used for trees generation. The trees were visualized using iTOL tool (https://itol.embl.de/). The analysis of BTN2 CR alleles in Yonemitsu et al. 2019 revealed that they are recombinant molecules with the insertion of M-mtDNA segment into the F-mtDNA. Therefore we employed the RDP4 package[46] to detect possible recombination breakpoints in the cancer-associated CR alleles found in our study (see Supplementary Fig. S5 caption for details).

In the comparative analyses of *M. trossulus* and BTN COI sequences, we considered the data from this study (four cancerous and 20 healthy mussels), those from previous BTN studies summarized by Yonemitsu et al. (2019) and all publically available *M. trossulus* COI data[10,33,47–50,51,52]. The alignment was created by ClustalW algorithm in MEGA X[43]. COI haplotype diversity was visualized using the TCS haplotype network[53] built within the PopART software[54]. *M. trossulus* samples were classified by their geographical origin into the western Pacific, eastern Pacific, western Atlantic and eastern Atlantic ones.

Species confirmation and sex identification

According to a recent survey[55], the regional blue mussel populations are overwhelmingly dominated by *M. trossulus*, but the presence of a "cryptic" species, *M. galloprovincialis*, and its hybrids with *M. trossulus* cannot be entirely ruled out. Mussels from the "I" sample (N=21), including four target mussels with DN, were genotyped for three nuclear markers routinely used for *M. trossulus* and *M. galloprovincialis* identification[56]: ME15/16[57], ITS[58] and MAL-I[59]. The

primers and protocols for amplification and interpretation of genotypes were as in original article. The DNA extracted from the hemolymph and from the mantle of each mussel was analyzed in parallel. The mussels were also sexed, at first by a microscopic examination of fresh tissues of the mantle, where the gonads in blue mussels are partly localized. It turned out, however, that most mussels were in post-spawned condition and lacked gametes. Therefore we identified their ~~"m~~itochondrial" sex by the presence or the absence of M-mtDNA 16S haplotypes, following the approach of Rawson and Hilbish (1995) and using DNA extracted from the mantle.

Results

DN diagnostics

Flow cytometry

Flow cytometry revealed two distinct patterns (Fig. 2). Most of the individuals had one peak of hemocytes, interpreted as diploid (Fig. 2a), or a diploid peak with a small admixture of tetraploids (Fig. 2b). These mussels were diagnosed as healthy. The second pattern was revealed in 10 ~~"J~~" individuals (4% of ~~"J~~" sample), which had an additional population of aneuploid cells (Fig. 2c-f). Their ploidy, calculated relatively to the 2n peak, varied among individuals from 3.7n to 5.2n. The ratio of these cells in the hemolymph of different mussels varied from 12 to 98%. These mussels were classified as ~~"D~~N-suggested". We did not reveal any significant signal from proliferating neoplastic cells, which could be expected as the third peak at the right side of the aneuploid peak at the histogram. Two ~~"D~~N suggested" mussels with a moderate ratio of neoplastic hemocytes, J54 (ratio 44.4%, ploidy 4.8n) and J111 (26.4%, 4.9n), and two mussels with a high ratio of neoplastic hemocytes, J161 (91%, 4.5n) and J181 (80%, 4.7n) (see Fig. 2c-f), were chosen for further analyses along with the control V1.

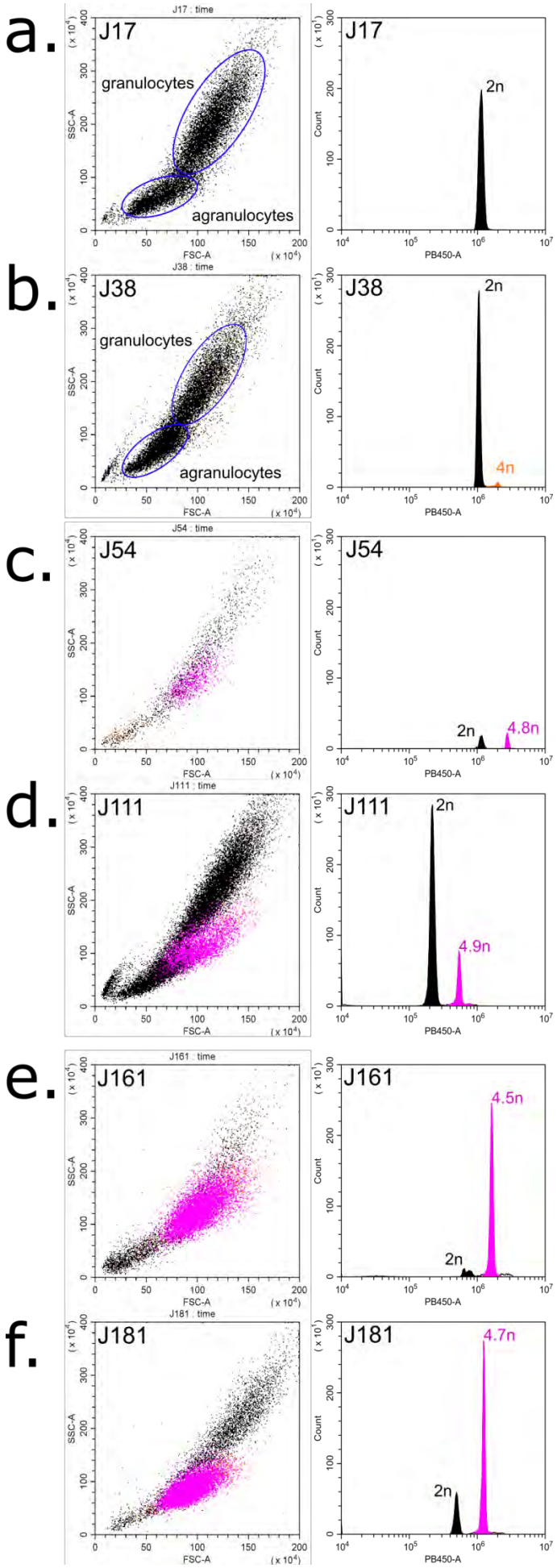

Figure 2. DN diagnostics in *M. trossulus* from the Gaydamak Bay, the Sea of Japan, by flow

cytometry. Flow cytometry plots depict cell groups (left graphs) and histograms revealing ploidy levels (right graphs) for healthy (**a, b**) and DN-suggested (**c-f**) mussels. An additional population of aneuploid cells (violet peaks and dots) is observed in the hemolymph of each DN-suggested mussel. Normal non-proliferating hemocytes are shown in black, normal proliferating hemocytes (tetraploid), in orange. Relative ploidy levels are given near the peaks. Subpopulations of agranulocytes and granulocytes are highlighted for healthy mussels (**a, b**). Individual numbers of mussels are given near the plots.

Hemocytology and immunochemistry

Hemocytological study revealed striking differences between the control mussels on the one hand and all the four DN-suggested mussels on the other hand. DN-suggested individuals had, in addition to normal adherent hemocytes with a low nucleus-to-cytoplasm ratio, also anomalous round non-adherent hemocytes. They looked like hedgehogs on the slides, the resemblance being due to an altered cytoskeleton with prominent actin ~~–s~~pikes". Their nuclei were pleomorphic, 3-4 times larger than those of normal hemocytes (Fig. 3). We considered these cells as neoplastic and the mussels they belonged to as DN-confirmed.

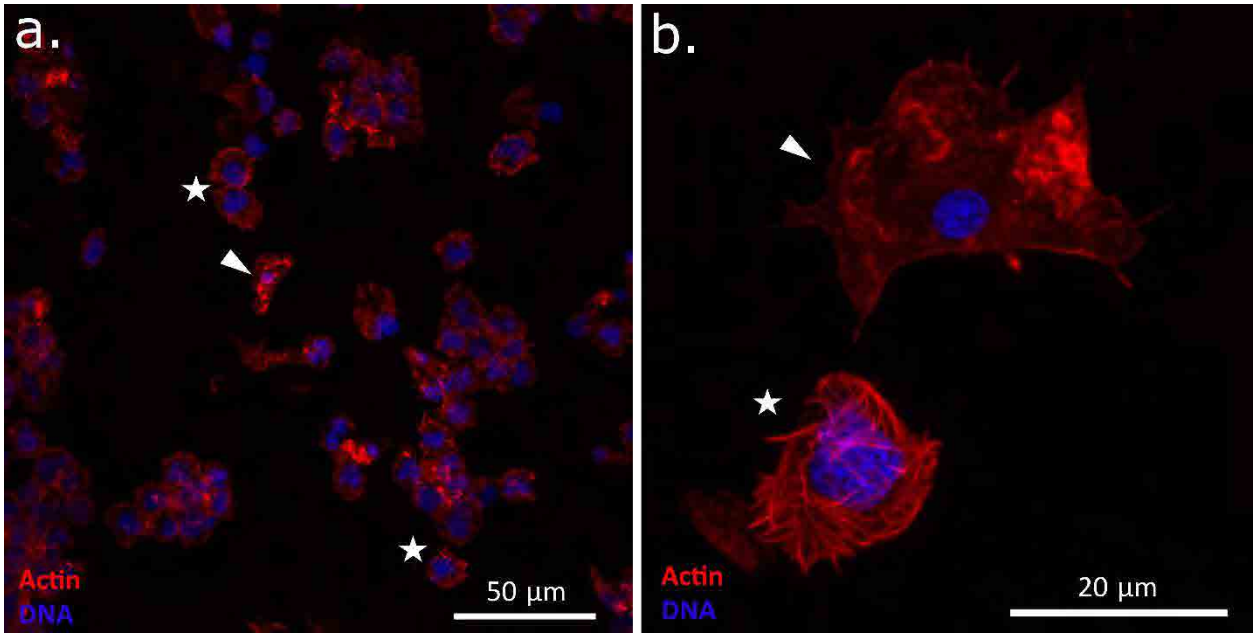

Figure 3. Confocal microscopy images of hemocytes of a DN-suggested mussel (J54) stained with DAPI (blue) and TRITC-labeled phalloidin (red). Images (**a**, **b**) are at two different magnifications (note the scale bars). Arrowheads point to normal adherent hemocytes with a small compact nucleus. Stars mark neoplastic aneuploid round cells with a large lobed nucleus and an altered actin cytoskeleton.

PCNA staining revealed few neoplastic hemocytes at the DNA synthesis stage (Supplementary Fig. S1). This observation was in line with the results of flow cytometry, which showed a low proliferating rate of the neoplastic cells.

BTN diagnostics

We managed to amplify one of the microsatellite markers, *Mg*µ3. The fragment size varied in the range of 141-146 bp. In healthy specimens (J2-J17, J38) the size and the representation of the amplified fragments (position and height of the peaks on the electropherograms, Supplementary Fig. S2, see also Fig. 1) from the hemolymph and from the foot samples were the same. In contrast, in all the four DN-confirmed mussels the 146 bp fragment was overrepresented in the hemolymph samples in comparison with the foot samples (Fig. 1, Supplementary Fig. S2). At the same time, this fragment, as well as the 144 bp fragment, characteristic of all the cancerous mussels, was also recorded in some healthy mussels, making the results inconclusive.

The final length of the sequences used for alignment was 447-453 bp for EF1α, 622-624 bp for CR and 630 bp for COI. The cloning results are summarized in supplementary Table S2**.** The NCBI GenBank accession numbers are given in Table S3. Hereafter the alleles identified in our study will be designated by letters if recorded in the study of Yonemitsu et al. 2019 and by numerals if newly found, except in a few cases when we wanted to emphasize the similarity between the alleles (e.g. EF1α-G1, CR-1‘, see below). It should be noted, however, that the alignments in Yonemitsu et al. (2019) were slightly longer than here.

The sequencing and molecular cloning of EF1α PCR products revealed identical sequences in the hemolymph and the foot tissues of the control individuals (see Supplementary Table S2 and Fig. 1). In contrast, all EF1α sequencing chromatograms from the hemolymph and the foot samples of DN-confirmed mussels showed a mixed signal. Molecular cloning of these PCR products revealed 2-4 different sequences in the foot samples and 2-6 different sequences in the hemolymph samples (Fig. 1; sequences found in one or just a few colonies are not considered). The diversity of sequences and their representation (numbers of colonies containing them) are illustrated in Supplementary Fig. S3. Some sequences were common, that is, represented in relatively many colonies, and differed by more than one substitution, while others were rare. All the mussels had two common sequences, EF1α-G and EF1α-H. They differed by 21 substitutions, which made them the most dissimilar common sequences, and were always more frequent in the hemolymph than in the foot samples. Other common sequences were usually specific of individual mussels and were present in both tissues (Fig. 1, Supplementary Table S2 and Supplementary Fig. S3). EF1α-G and EF1α-H putatively represented heterozygous cancer genotype. Other common sequences probably represented the diploid genomes of the host. Rare sequences, including EF1α-G1 different from EF1α-G by one substitution (Supplementary Fig. S3), were probably methodological artifacts.

Direct sequencing of COI and CR revealed identical alleles in the hemolymph and in the foot samples of individual control mussels, in homoplasmic condition (J17 and J38, Supplementary Table S2). On the contrary, the chromatograms from analyses of different tissues of mussels with DN looked very different.

No heteroplasmy was observed on the CR chromatograms of cancerous mussels. Unique alleles were identified in the foot samples. Altogether, two alleles were identified in the hemolymph samples: CR-1 in J54 and J161 and CR-2 in J111 and J181. CR-1 and CR-2 were very different both from each other (31 substitutions, 5.0% difference) and from the other alleles (2.7-6.6%), considering that the differences between all the other alleles were within the range of 0.3-1.5%. Molecular cloning confirmed the results of direct sequencing, but also revealed rarer sequences invisible on sequencing chromatograms (Supplementary Table S2, Fig. 1). In the hemolymph of J111 and J181 the same alleles as in foot were found, while in the hemolymph of J161 allele CR-1‘, supported by five clones, was found, differing from the major CR-1 allele by four substitutions.

No COI heteroplasmy was observed in the foot samples of cancerous mussels while several positions with overlapping peaks of a very different height were observed on chromatograms of the hemolymph samples (cf. Fig. 1). The sequences of additional alleles were easily reconstructed by comparing the chromatograms: the minor peaks were from the ―foot alleles” of the same mussels. Two major COI sequences were identified in the hemolymph samples: COI-1 in J54 and J161 and COI-2 in J111 and J181. These alleles differed from each other by 6 substitutions (0.95%) and by 0.60-0.95% from all the other alleles.

Thus, the sequence analyses revealed genetic chimerism of mussels with DN, with the hemolymph and the foot tissues being dominated by different genotypes. However, while EF1α genotyping revealed the same cancer genotype in all the diseased mussels, mtDNA genotyping revealed two different cancer genotypes, marked by different combinations of COI and CR alleles, in different mussels. The conclusive evidence that DN in mussels from the Sea of Japan is BTN came from the genetic comparison with the previously studied cancers.

Phylogenetic analysis

Maximum likelihood trees

A general inspection of phylogenetic trees (Fig. 4) shows that the Sea of Japan mussels are infected with BTN2. EF1α-G and EF1α-H cancerous alleles identified in them are known BTN2-specific alleles. For both mtDNA fragments the cancerous alleles clustered together with the major BTN2-specific alleles and the 62mc10 (Fig. 4). COI-1 and COI-2 differed from the major

COI-B BTN2 allele by 6 and 8 substitutions, respectively. CR-1 allele differed from the closest CR-D allele by 16 substitutions, and from the 62mc10 by 11 substitutions. CR-2 differed from the closest CR-C allele by 5 substitutions. The alleles of *M. trossulus* (i.e. host alleles) from the Sea of Japan were randomly scattered across the *M. trossulus* clade on the trees (Fig. 4). Only one of these alleles, EF1α-D, has been identified before.

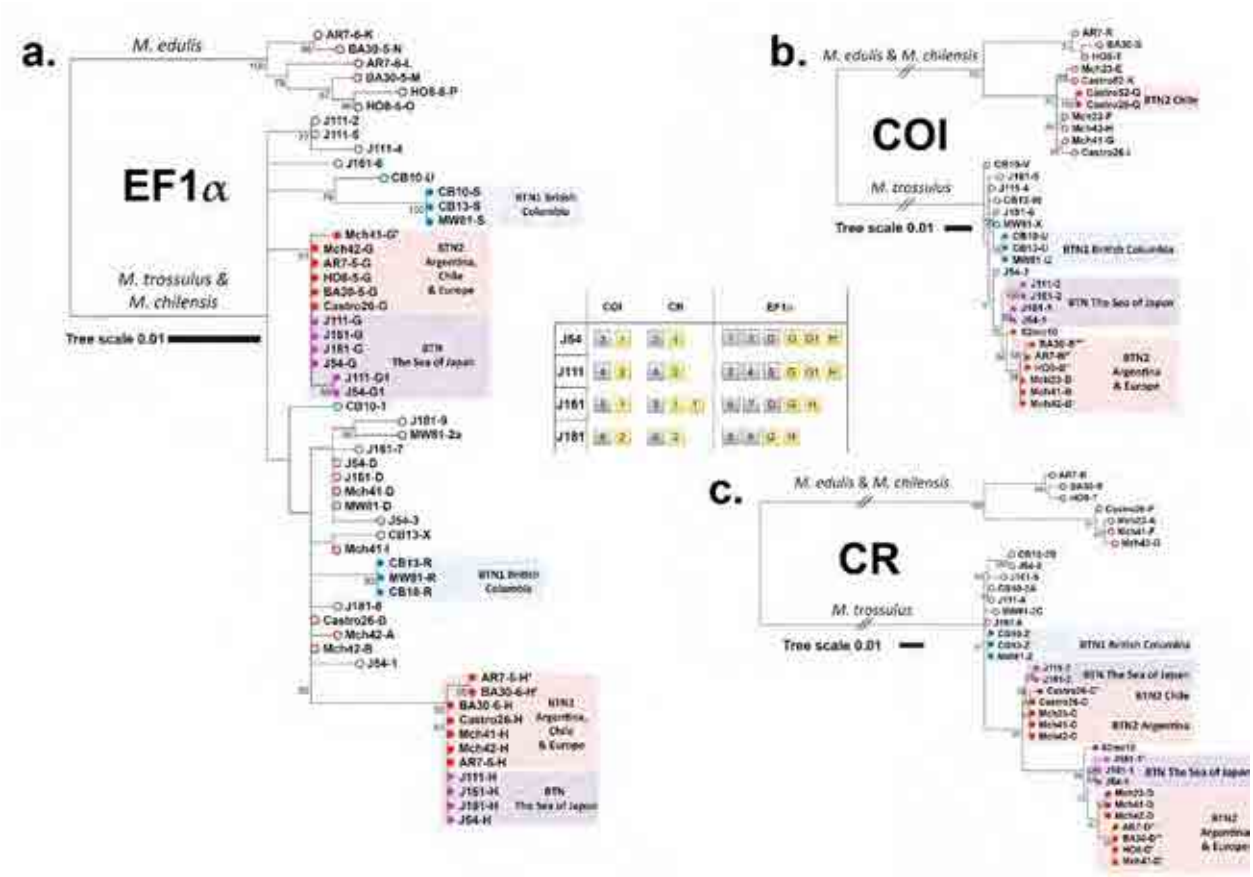

Figure 4. Phylogenetic analysis of nuclear and mitochondrial loci from mussels with BTN. (**a**) EF1α maximum likelihood tree based on the 629 bp alignment (HKY85+G substitution model) (**b**) COI maximum likelihood tree based on the 630 bp alignment (GTR+G substitution model) (**c**) CR maximum likelihood tree based on the 842 bp alignment (HKY+G substitution model). Maximum likelihood trees were rooted at the midpoint, with bootstrap values below 50 removed. Branches marked by two slashes were shortened 5-fold for COI and 3-fold for CR. The scale bars mark genetic distance. Source data include all references from Yonemitsu et al. (2019) with original allele nomenclature (specimen ID, allele ID; Castro26 host COI allele J not included because of the short length of sequence), mitochondrial sequence KM192133 from the Baltic mussel 62mc10 and new data on four mussels with DN from the Sea of Japan. Open circles at the end of branches mark host alleles, closed circles mark cancer alleles. Alleles revealed in mussels with BTN1 are marked in blue, those revealed in mussels with BTN2, in red. Alleles revealed in mussels from the Sea of Japan are marked in violet (alleles are listed in the legend).

Geographic origin of the samples and species identity of clades are indicated. Alignments are provided in Supplementary data S1-S3.

An analysis of recombination identified the same breakpoints in CR-1/CR-1‘ and CR-D alleles but different breakpoints in CR-2 and CR-C alleles (see Supplementary Fig. S5). However, CR-2 and CR-C differed by only two substitution between the suggested breakpoints. We will therefore adhere to the hypothesis that CR-1 and CR-D, as well as CR-2 and CR-C, represent the same mitochondrial lineages originated through singular recombination events. To remember, individual J161 was heteroplasmic for the close CR-1 and CR-1‘ alleles. Such ―additional" heteroplasmy occasionally occurs in BTN2 in different parts of its geographical distribution (Mch-41, Castro-26, Fig. 5).

In addition to the genetic similarity of BTN2 worldwide, Fig. 4 also illustrates geographic differences within this cancer. Apart from the originality of the Chilean cancer clones (Castro26), the differences are as follows. In the Sea of Japan there are basically two cancer mtDNA haplotypes, comprising two 1% divergent COI alleles and two very divergent CR alleles (CR-1, CR-2), while elsewhere there are two cancer haplotypes, comprising basically the same COI alleles of the ―B group" and two CR alleles (CR-C, CR-D) very similar to that in the Sea of Japan. Another difference is that the two cancer haplotypes are apparently homoplasmic in the Sea of Japan and in Europe but heteroplasmic in Argentine (both alleles in the same cancerous mussels).

Haplotype network

Among the data sets included in the analysis, that from Vancouver Island in British Columbia in Eastern Pacific[49] demonstrated a remarkable polymorphism in comparison with other regional sets, including that from the same macroregion. Therefore we provide separate networks performed with and without data of Crego-Prieto et al., 2015 in Fig. 5 and Supplementary Fig. S4, respectively. The analysis revealed a complex star-like haplotype network familiar from the previous phylogeographic studies[31,48,60]. The network consisted of several major clades, each composed of a common core haplotype and many rare haplotypes radiating from it. Some clades were ―cosmopolitan" and included samples from both the Atlantic and the Pacific oceans, while others included samples almost only from the Pacific. The BTN1 unique allele belonged to one of the cosmopolitan clades. It included sequences from all the four macroregions considered but was dominated by samples from eastern Pacific. The BTN2 alleles, including that from the Sea of Japan, and the Baltic 62mc10, joined the other clade. This clade included samples from all macroregions but eastern Pacific (Fig. 5), with one notable exception. A single sequence

identical to the cancerous COI-1 from the Sea of Japan was identified in the data from Bamfield

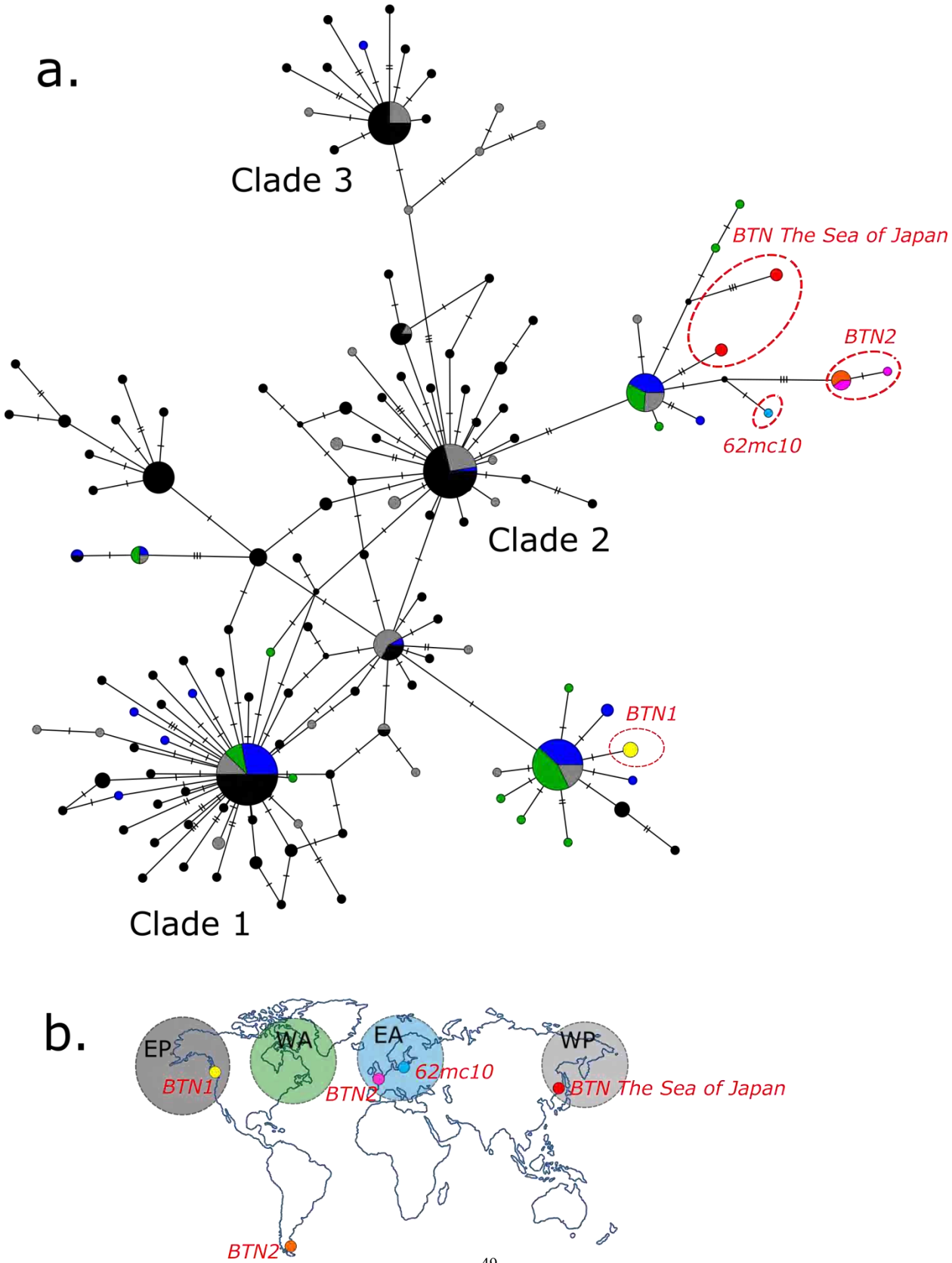

locality on Vancouver Island (NCBI KF931805.1[49], Supplementary Fig. S4).

Figure 5. (**a**) *M. trossulus* and BTN COI haplotype network obtained from the TCS analysis. The analysis was based on the 542 bp long alignment (provided as Supplementary data S4) of 350 sequences produced in this study (4 cancerous and 20 healthy mussels), from previous BTN studies together with all publically available *M. trossulus* sequences (see the list of sequences in Supplementary Table S1). Each circle represents a single allele. The size of the circle is proportional to the number of individuals bearing the allele. Bars indicate mutations between alleles. Small black circles indicate hypothetical haplotypes predicted by the model. The geographical origin of samples is color-coded and illustrated in the map (**b**). Samples corresponding to BTN1 (all from British Columbia) are in yellow, to BTN2, in pink (Europe) and orange (Argentine), to BTN from the Sea of Japan, in red. Reference *M. trossulus* samples from West Pacific (WP on the map) are in grey, from East Pacific (EP), in black, from West Atlantic (WA), in green, from East Atlantic (EA), in dark blue, and from the Baltic Sea (a single 62mc10 sample), in light blue. Clades 1-3 are named after Marko et al. (2010). See Supplementary Fig. S4 for the results of a re-analysis of these data together with those from Crego-Prieto et al. (2015).

Species confirmation and sex identification

Only *M. trossulus* alleles were recorded in a subsample of mussels (N=21, including J17, J38, and cancerous J54, J111, J161 and J181) studied by three additional nuclear markers, and the genotypes retrieved from different tissues of the same mussels were always the same. Twelve mussels were identified as ~~"m~~itochondrial males" by 16s locus, among them J181, and the other mussels, as females.

Discussion

In this study we showed that *Mytilus trossulus* mussels from the Sea of Japan were affected with DN and confirmed that it was caused by CTC by demonstrating genetic chimerism of mussels with DN and a striking similarity of their ~~"e~~xtra" genotypes. The cancer alleles found in our study did not match those of BTN1 from *M. trossulus* populations at the American coast of the Pacific Ocean but matched the alleles of BTN2 lineage, previously diagnosed in *M. edulis* from Europe and in *M. chilensis* from Chile and Argentine but not in *M. trossulus*, from which it derived. So, we assume that *M. trossulus* from the Sea of Japan are infected by BTN2. Our finding means that this species, contrary to the hypothesis of Yonemitsu et al. (2019), has not evolved resistance to this disease. Below we will first discuss the pathology and epidemiology of BTN2 in mussels from the Sea of Japan and then its genetic properties.

The features of the neoplastic hemocytes in our study—a rounded shape, a large nucleus (3-4 times larger than in normal hemocytes), a high nucleus-to-cytoplasm ratio and an increased ploidy—agree with the previous descriptions of DN in *Mytilus*[14,22,23]. What seems unusual is their low proliferation level. Neoplastic hemocytes of mussels are generally assumed to have a high proliferation activity[20]. However, a low proliferation rate of neoplastic hemocytes in

453 mussels with DN was reported in two other studies: that of Burioli et al. (2019) who studied
454 BTN (supposedly BTN2) in France and that of Cremonte et al. (2011) who studied DN in the
455 same Argentinean population where BTN2 was later recognized by Yonemitsu et al. (2019). A
456 possible explanation is that in case of BTN2 the proliferation site of the neoplastic cells is
457 located not in the hemolymph. This hypothesis is inspired by the study of Burioli et al. (2019),
458 who observed a high mitotic rate of neoplastic cells in the vesicular connective tissue of BTN-
459 infected mussels.

460 Our data complement the results of another study of DN in mussels from the Sea of Japan[36],
461 whose authors found only one individual with DN after a histological examination of 40
462 mollusks from various localities. We found DN in a single population from the Gaydamak Bay.
463 Our values of DN prevalence in it (4.0%) were probably underestimated, being based on flow
464 cytometry, which is not very sensitive at the early stages of the disease[19,22]. In the study of DN in
465 *M. trossulus* from British Columbia[19] flow cytometry was quite reliable at the late stages but
466 detected only 30% of the early stages diagnosed by hemocytology. As a result, the overall
467 prevalence based on flow cytometry was underestimated two-fold[19]. Still, our estimate of DN
468 level in the population from the Gaydamak Bay is close to the mean prevalence of DN reported
469 for *Mytilus* populations worldwide[35,61–64] and much lower than the maximal prevalence of 56%
470 reported for *M. trossulus* population from British Columbia[65].

471 Noteworthy, the mussels in the Gaydamak Bay were collected from the surface of a mooring
472 buoy in a heavily polluted area, where no mussels were recorded at the sea floor (our
473 observations). Since BTN is presumably transmitted by cancer cells through the water column,
474 we suspect that the mussels fouling the buoy contracted the infection from those that had fouled
475 ships moored to it. We point out that mussel populations on mooring buoys, docks etc. may serve
476 as BTN reservoirs while mussel-fouled ships may be the vectors of the disease.

477 An association between an increased prevalence of DN in mollusks and a high concentration of
478 pollutants, though often surmised, has never been shown explicitly[24]. Our samples from other
479 localities than Gaydamak were limited, and we have no reasons to suppose that mussel
480 populations outside harbors in the Sea of Japan are free from the disease. *M. trossulus*
481 populations in the Sea of Japan and in West Pacific in general may be a natural reservoir of
482 BTN2, where it is maintained and whence it spreads worldwide.

483 We obtained four BTN2 genotypes, in addition to 11 cancers, eight of them representing BTN2,
484 studied earlier[2,10]. We confirm the conclusions of Yonemitsu et al. (2019) that BTNs are marked
485 by lineage-specific genotypes at the conservative nuclear EF1α locus and that mitochondrial

diversity is observed across BTN2 clones from different individuals as well as within some clones. This diversity is difficult to interpret at the moment, firstly because of the lack of data and secondly because of the possibility of mitochondrial capture from the host and mitochondrial recombination[10,30,66].

Two main mitochondrial haplotypes defined as combinations of COI and CR alleles COI-1+CR-1 and COI-2+CR-2 found in homoplasmic condition in our material were similar but not identical to the two common cancer-associated haplotypes combining the COI-B alleles and the CR alleles D and C, respectively, revealed by Yonemitsu et al. (2019) either in heteroplasmic (Argentine) or homoplasmic (Europe, CR-D allele) state.

Noteworthy, the homoplasmy of mussel cancers from the Sea of Japan might be spurious. Yonemitsu et al. (2019) has shown using qPCR that the levels of various haplotypes in heteroplasmic cancer clones may be very different. Since we employed molecular cloning of CR and sequenced a limited numbers of colonies (though more than Yonemitsu et al. (2019) did to demonstrate heteroplasmy), we might have overlooked rare alleles. Further, if we assume that the cancer clones from Gaydamak are homoplasmic, it follows that the mussels fouling the same mooring buoy were infected with at least two independent clones, which is unlikely, though not impossible.

One new finding that emerged in our study is an increased divergence between haplotypes in the Sea of Japan. Two COI alleles differed from each other and from ~~"B~~ alleles", on the average, by six substitutions (~1%). This diversity has probably accumulated after the emergence of BTN2. In a study of CTVT mtDNA evolution, Strakova et al. (2017) considered three estimates of mutation rates (mutations per year): based on CTVT nuclear phylogeny (maximum rate estimate 0.0205), based on the tempo of accumulation of mutations by human cancers with patient age (0.025) and based on cell divisions adjusted for CTVT generation time (0.0183-0.0913). Employing these rates to the 640 bp long COI fragment and assuming that each main BTN2 COI lineage acquired on the average three mutations through evolution, we obtain the divergence time estimates of 3849, 3156 and 865-4323 years, respectively. These estimates can hardly be accurate since COI is a relatively slow-evolving region of the mitochondrial genome[67] and mutational rates in *Mytilus* are faster than in *Canis*[68,69]. At the same time, mitochondrial mutation rates and generation time in BTNs are unknown. A cautious conclusion would be that BTN2 emerged long before DN was first diagnosed in blue mussels in the 1960s[15].

As for the geographical origin of the BTN2 COI diversity, the comparison with a rich collection of *M. trossulus* COI sequences indicates that it most probably lies outside the East Pacific.

Intriguingly, the unique COI allele of the other cancer lineage, BTN1, so far revealed only in British Columbia[10], belongs to the haplogroup that is much more common in the Atlantic and the West Pacific than in the East Pacific. Hence our analysis did not confirm unambitiously the endemism of BTN1 to the East Pacific (Fig. 5).

At least two of the published *M. trossulus* sequences considered in our analyses could turn out to be cancer genotypes. One of them is COI KF931805 from Vancouver Island in British Columbia[49], which is identical to BTN2 allele COI-2. This might mean that BTN2 is cryptically present in British Columbia. If so, DN in mussels from this region could be caused by both BTN1 and BTN2.

Another candidate for a cancerous sequence is KM192133 from the Baltic Sea (genome 62mc10)[33], which closely matches BTN2 haplotypes (Fig. 4). Yonemitsu et al. (2019) considered 62mc10 as a genome of ~~a~~ normal *M. trossulus* from the Baltic region", which is close to the ancestral sequence of BTN2, rather than the genome of the cancer itself. There are, however, several reasons to consider the possibility that 62mc10 might be cancerous. Firstly, *M. trossulus* from the Baltic generally lack their native mtDNA. It was replaced by *M. edulis* mtDNA as a consequence of introgressive hybridization between these species[70,71]. In fact, 62mc10 is the only *M. trossulus* mitochondrial sequence revealed in extensive studies of the Baltic mussels[33]. Secondly, 62mc10 was identified in the mantle (i.e. the gonad) of a female alongside with the standard *M. edulis* F-mtDNA[33]. At the same time, 62mc10, as well as BTN2 mtDNA, is a mosaic sequence: F-mtDNA with M-mtDNA CR segments[10,33]. In mussels, such recombinant mtDNA are usually inherited as standard M-mtDNA (~~m~~masculinized" genomes) and so are expected to be found, in a mixture with the F-mtDNA, in gonads of males, not females[47,72]. The mantle tissues are subject to cancer[14], which can explain the heteroplasmy, and DN has indeed been recorded in the Baltic Sea *M. trossulus*[35].

The origin of the two cancerous complex mitochondrial haplotypes—so original in their control regions and so similar in their coding parts, occurring sometimes together and sometimes apart—remains enigmatic. There is little we can add on this matter to the discussion in Yonemitsu et al. (2019). BTN2 haplotypes resemble the recombinant ~~m~~masculinized" genomes (see above). These genomes are common in the Baltic mussels, in which they are *M. edulis*-derived (with the sole exception of 62mc10) and in the hybrid zone between *M. edulis* and *M. trossulus* in Norway, in which they are *M. trossulus*-derived, but rare elsewhere[34,73]. Recombination and masculinization in the Baltic and in Norway are thought to be driven by hybridization between *M. edulis* and *M. trossulus*[33,34]. The ubiquity of masculinized genomes in these two regions prompted Yonemitsu et al. (2019) to suggest that BTN2 originated in one of them. If this hypothesis is true, more

553 extensive genetic surveys would find traces of introgression from *M. edulis* in BTN2 nuclear
554 genome. For example, the absolute majority of the Baltic mussels bear *M. edulis* alleles at the
555 ITS multicopy gene[74]. The lack of *M. edulis* ITS alleles in the hemolymph of cancerous mussels
556 from the Sea of Japan in our study is an additional though not conclusive argument against the
557 Baltic origin of BTN2. While the European origin of BTN2 cannot be refuted, we suggest an
558 alternative hypothesis that it emerged in the heart of *M. trossulus* ancestral range in the West
559 Pacific.

560 The similarity between BTN2 and ~~"m~~masculinized" mtDNA might indicate not only the
561 population of the BTN2 origin but also the tissue where it originated and the sex of ~~"p~~atient
562 zero", the mussel from which BTN2 derive. During embryonic development, paternally inherited
563 mtDNA are maintained in the germline of males[75], being the genetic marker of male germ cells.
564 This could mean that cancer cells are male germ cells but not hemocytes by origin. If this is true,
565 the first mussel with BTN2 was a male.

566 # References

567 1. Murchison, E. P. Clonally transmissible cancers in dogs and Tasmanian devils. *Oncogene*
568 **27**, S19–S30 (2008).

569 2. Metzger, M. J. *et al.* Widespread transmission of independent cancer lineages within
570 multiple bivalve species. *Nature* **534**, 705–709 (2016).

571 3. Storfer, A. *et al.* The devil is in the details: Genomics of transmissible cancers in
572 Tasmanian devils. *PLoS Pathog.* **14**, 1–7 (2018).

573 4. Nowinsky, M. A. Zur Frage ueber die Impfung der krebsigen Geschwuelste. *Zentralbl*
574 *Med Wissensch.* **14**, 790–791 (1876).

575 5. Murgia, C., Pritchard, J. K., Kim, S. Y., Fassati, A. & Weiss, R. A. Clonal Origin and
576 Evolution of a Transmissible Cancer. *Cell* **126**, 477–487 (2006).

577 6. Pearse, A. M. & Swift, K. Allograft theory: Transmission of devil facial-tumour disease.
578 *Nature* **439**, 549 (2006).

579 7. Siddle, H. V. *et al.* Transmission of a fatal clonal tumor by biting occurs due to depleted
580 MHC diversity in a threatened carnivorous marsupial. *Proc. Natl. Acad. Sci. U. S. A.* **104**,
581 16221–16226 (2007).

582 8. Metzger, M. J. J., Reinisch, C., Sherry, J. & Goff, S. P. P. Horizontal transmission of

clonal cancer cells causes leukemia in soft-shell clams. *Cell* **161**, 255–263 (2015).

9. Riquet, F., Simon, A. & Bierne, N. Weird genotypes? Don‘t discard them, transmissible cancer could be an explanation. *Evol. Appl.* **10**, 140–145 (2017).

10. Yonemitsu, M. A. *et al.* A single clonal lineage of transmissible cancer identified in two marine mussel species in South America and Europe. *Elife* **8**, 1–21 (2019).

11. Woods, G. M., Bruce Lyons, A. & Bettiol, S. S. A devil of a transmissible cancer. *Trop. Med. Infect. Dis.* **5**, 1–10 (2020).

12. Ganguly, B., Das, U. & Das, A. K. Canine transmissible venereal tumour: A review. *Vet. Comp. Oncol.* **14**, 1–12 (2016).

13. Paynter, A. N., Metzger, M. J., Sessa, J. A. & Siddall, M. E. Evidence of horizontal transmission of the cancer-associated Steamer retrotransposon among ecological cohort bivalve species. *Dis. Aquat. Organ.* (2017). doi:10.3354/dao03113

14. Barber, B. J. Neoplastic diseases of commercially important marine bivalves. *Aquat. Living Resour.* **17**, 449–466 (2004).

15. Farley, C. A. Sarcomatoid proliferative disease in a wild population of blue mussels (*Mytilus edulis*). *J. Natl. Cancer Inst.* **43**, 509–516 (1969).

16. Sparks, A. K. *Synopsis of Invertebrate Pathology Exclusive of Insects*. (Elsevier, 1985).

17. Muttray, A. F. & Vassilenko, K. Mollusca: Disseminated Neoplasia in Bivalves and the p53 Protein Family. *Adv. Comp. Immunol.* 953–979 (1969). doi:10.1007/978-3-319-76768-0

18. Bihari, N., Mičić, M., Batel, R. & Zahn, R. K. Flow cytometric detection of DNA cell cycle alterations in hemocytes of mussels (*Mytilus galloprovincialis*) off the Adriatic coast, Croatia. *Aquat. Toxicol.* **64**, 121–129 (2003).

19. Vassilenko, E. & Baldwin, S. A. Using flow cytometry to detect haemic neoplasia in mussels (Mytilus trossulus) from the Pacific Coast of Southern British Columbia, Canada. *J. Invertebr. Pathol.* **117**, 68–72 (2014).

20. Moore, J. D., Elston, R. A., Drum, A. S. & Wilkinson, M. T. Alternate pathogenesis of systemic neoplasia in the bivalve mollusc *Mytilus*. *J. Invertebr. Pathol.* **58**, 231–243 (1991).

21. Benabdelmouna, A., Saunier, A., Ledu, C., Travers, M. A. & Morga, B. Genomic

abnormalities affecting mussels (*Mytilus edulis-galloprovincialis*) in France are related to ongoing neoplastic processes, evidenced by dual flow cytometry and cell monolayer analyses. *J. Invertebr. Pathol.* **157**, 45–52 (2018).

22. Burioli, E. A. V *et al.* Implementation of various approaches to study the prevalence , incidence and progression of disseminated neoplasia in mussel stocks. **168**, (2019).

23. Moore, C. A., Beckmann, N. & Patricia Morse, M. Cytoskeletal structure of diseased and normal hemocytes of *Mya arenaria*. *J. Invertebr. Pathol.* **60**, 141–147 (1992).

24. Carballal, M. J., Barber, B. J., Iglesias, D. & Villalba, A. Neoplastic diseases of marine bivalves. *J. Invertebr. Pathol.* (2015). doi:10.1016/j.jip.2015.06.004

25. Odintsova, N. A. Leukemia-Like Cancer in Bivalves. *Russ. J. Mar. Biol.* (2020).

26. Smolowitz, R. M. & Reinisch, C. L. Indirect peroxidase staining using monoclonal antibodies specific for *Mya arenaria* neoplastic cells. *J. Invertebr. Pathol.* **48**, 139–145 (1986).

27. McDonald, J. H., Seed, R. & Koehn, R. K. Allozymes and morphometric characters of three species of *Mytilus* in the Northern and Southern Hemispheres. *Mar. Biol.* **111**, 323–333 (1991).

28. Larraín, M. A., Zbawicka, M., Araneda, C., Gardner, J. P. A. & Wenne, R. Native and invasive taxa on the Pacific coast of South America: Impacts on aquaculture, traceability and biodiversity of blue mussels (*Mytilus* spp.). *Evol. Appl.* **11**, 298–311 (2018).

29. Pye, R. J. *et al.* A second transmissible cancer in Tasmanian devils. *Proc. Natl. Acad. Sci. U. S. A.* **113**, 374–379 (2016).

30. Strakova, A. *et al.* Mitochondrial genetic diversity, selection and recombination in a canine transmissible cancer. *Elife* **5**, 1–25 (2016).

31. Rawson, P. D. & Harper, F. M. Colonization of the northwest Atlantic by the blue mussel, *Mytilus trossulus* postdates the last glacial maximum. *Mar. Biol.* **156**, 1857–1868 (2009).

32. Wenne, R., Bach, L., Zbawicka, M., Strand, J. & McDonald, J. H. A first report on coexistence and hybridization of *Mytilus trossulus* and *M. edulis* mussels in Greenland. *Polar Biol.* **39**, 343–355 (2016).

33. Zbawicka, M., Wenne, R. & Burzyński, A. Mitogenomics of recombinant mitochondrial genomes of Baltic Sea *Mytilus* mussels. *Mol. Genet. Genomics* **289**, 1275–1287 (2014).

643 34. Śmietanka, B. & Burzyński, A. Disruption of doubly uniparental inheritance of
644 mitochondrial DNA associated with hybridization area of European *Mytilus edulis* and
645 *Mytilus trossulus* in Norway. *Mar. Biol.* 164–209 (2017). doi:10.1007/s00227-017-3235-5

646 35. Sunila, I. Histopathology of mussels (*Mytilus edulis* L.) from the Tvarminne area, the Gulf
647 of Finland (Baltic Sea). *Ann. Zool. Fennici* (1987).

648 36. Usheva, L. N. & Frolova, L. T. Neoplasia in the connective tissue tumor in the mussel
649 *Mytilus trossulus* from a polluted region of Nakhodka Bay, the Sea of Japan. *Ontogenez*
650 **31**, 63–70 (2000).

651 37. Maiorova, M. A. & Odintsova, N. A. β integrin-like protein-mediated adhesion and its
652 disturbances during cell cultivation of the mussel Mytilus trossulus. *Cell Tissue Res.* **361**,
653 581–592 (2015).

654 38. Marigomez, I., Lekube, X. & Cancio, I. Immunochemical localisation of proliferating
655 cells in mussel digestive gland tissue. *Histochem. J.* **31**, 781–788 (1999).

656 39. Maiorova, M. A. & Odintsova, N. A. Proliferative potential of larval cells of the mussel
657 <i>Mytilus trossulus<i> and their capacity to differentiate into myogenic cells in culture.
658 *Russ. J. Mar. Biol.* **42**, 281–285 (2016).

659 40. Voronezhskaya, E. E., Nezlin, L. P., Odintsova, N. A., Plummer, J. T. & Croll, R. P.
660 Neuronal development in larval mussel *Mytilus trossulus* (Mollusca: Bivalvia).
661 *Zoomorphology* **127**, 97–110 (2008).

662 41. Presa, P., Pérez, M., Diz, A. P., Perez, M. & Diz, A. P. Polymorphic microsatellite
663 markers for blue mussels (*Mytilus* spp.). *Conserv. Genet.* **3**, 441–443 (2002).

664 42. Zouros, E. Biparental Inheritance Through Uniparental Transmission: The Doubly
665 Uniparental Inheritance (DUI) of Mitochondrial DNA. *Evol. Biol.* **40**, 1–31 (2013).

666 43. Kumar, S., Stecher, G., Li, M., Knyaz, C. & Tamura, K. MEGA X: Molecular
667 Evolutionary Genetics Analysis across Computing Platforms. **35**, 1547–1549 (2018).

668 44. Paabo, S., Irwin, M. & Wilson, C. DNA Damage Promotes Jumping between Templates
669 during Enzymatic Amplification. *J. Biol. Chem.* **265**, 4718–4721 (1990).

670 45. Bradley, R. D. & Hillis, D. A. Recombinant DNA Sequences Generated by PCR
671 Amplification. *Mol. Biol. Evol.* **14**, 592–593 (1997).

672 46. Martin, D. P., Murrell, B., Golden, M., Khoosal, A. & Muhire, B. RDP4: Detection and

analysis of recombination patterns in virus genomes. *Virus Evol.* **1**, 1–5 (2015).

47. Breton, S., Burger, G., Stewart, D. T. & Blier, P. U. Comparative analysis of gender-associated complete mitochondrial genomes in marine mussels (*Mytilus* spp.). *Genetics* **172**, 1107–1119 (2006).

48. Marko, P. B. *et al.* The ‗Expansion-Contraction' model of Pleistocene biogeography: Rocky shores suffer a sea change? *Mol. Ecol.* **19**, 146–169 (2010).

49. Crego-Prieto, V., Juanes, F. & Garcia-Vazquez, E. Aquaculture and the spread of introduced mussel genes in British Columbia. *Biol. Invasions* (2015). doi:10.1007/s10530-015-0853-z

50. Chung, J. M. *et al.* Molecular phylogenetic study of bivalvia from four countries (China, Japan, Russia and Myanmar) using 3 types of primers. *Korean J. Malacol.* **35**, 137–148 (2019).

51. Layton, K. K. S., Martel, A. L., Hebert, P. D. N. & Layton, K. K. S. Patterns of DNA Barcode Variation in Canadian Marine Molluscs. *PLoS One* **9**, 1–9 (2014).

52. deWaard, J. R. *et al.* A reference library for Canadian invertebrates with 1.5 million barcodes, voucher specimens, and DNA samples. *Sci. Data* **6**, 1–12 (2019).

53. Clement, M., Snell, Q., Walker, P., Posada, D. & Crandall, K. TCS: Estimating Gene Genealogies. *Parallel Distrib. Process. Symp. Int.* **2**, (2002).

54. Leigh, J. W. & Bryant, D. POPART: Full-feature software for haplotype network construction. *Methods Ecol. Evol.* **6**, 1110–1116 (2015).

55. Kartavtsev, Y. P., Masalkova, N. A. & Katolikova, M. V. Genetic and Morphometric Variability in Settlements of Two Mussel Species (*Mytilus* ex. gr. *Edulis*), *Mytilus trossulus* and *Mytilus galloprovincialis* , in the Northwestern Sea of Japan. *J. Shellfish Res.* **37**, 103–119 (2018).

56. Larraín, M. A., González, P., Pérez, C. & Araneda, C. Comparison between single and multi-locus approaches for specimen identification in *Mytilus mussels*. *Sci. Rep.* **9**, 1–13 (2019).

57. Inoue, K., Waite, J. H., Matsuoka, M., Odo, S. & Harayama, S. Interspecific variations in adhesive protein sequences of *Mytilus edulis*, *M. galloprovincialis*, and *M. trossulus*. *Biol. Bull.* **189**, 370–375 (1995).

58. Heath, D. D., Rawson, P. D. & Hilbish, T. J. PCR-based nuclear markers identify alien blue mussel *Mytilus* spp. genotypes on the west coast of Canada. *Can. J. Fish. Aquat. Sci.* **52**, 2621–2627 (1995).

59. Rawson, P. D., Secor, C. L. & Hilbish, T. J. The effects of natural hybridization on the regulation of doubly uniparental mtDNA inheritance in blue mussels (*Mytilus* spp.). *Genetics* **144**, 241–248 (1996).

60. Laakkonen, H. M., Hardman, M., Strelkov, P. & Väinölä, R. Cycles of trans-Arctic dispersal and vicariance, and diversification of the amphi-boreal marine fauna. *J. Evol. Biol.* 1–24 (2020). doi:10.1111/jeb.13674

61. Ciocan, C. & Sunila, I. Disseminated neoplasia in blue mussels, *Mytilus galloprovincialis*, from the Black Sea, Romania. *Mar. Pollut. Bull.* **50**, 1335–1339 (2005).

62. Gombač, M., Sitar, R., Pogačnik, M., Arzul, I. & Jenčič, V. Haemocytic neoplasia in Mediterranean mussels (*Mytilus galloprovincialis*). *Mar. Freshw. Behav. Physiol.* **46**, 135–143 (2013).

63. Villalba, A., Mourelle, S. G., Carballal, M. J. & López, C. Symbionts and diseases of farmed mussels *Mytilus galloprovincialis* throughout the culture process in the Rias of Galicia (NW Spain). *Dis. Aquat. Organ.* **31**, 127–139 (1997).

64. Cremonte, F., Puebla, C., Tillería, J. & Videla, V. Estudio histopatológico del chorito *Mytilus chilensis* (Mytilidae) y del culengue Gari solida (Psammobiidae) en el sur de Chile. *Lat. Am. J. Aquat. Res.* **43**, 248–254 (2015).

65. Vassilenko, E. I., Muttray, A. F., Schulte, P. M. & Baldwin, S. A. Variations in p53-like cDNA sequence are correlated with mussel haemic neoplasia: A potential molecular-level tool for biomonitoring. *Mutat. Res. - Genet. Toxicol. Environ. Mutagen.* (2010). doi:10.1016/j.mrgentox.2010.06.001

66. Rebbeck, C. A., Leroi, A. M. & Burt, A. Mitochondrial capture by a transmissible cancer. *Science (80-.).* **331**, 303 (2011).

67. Pesole, G., Gissi, C., De Chirico, A. & Saccone, C. Nucleotide substitution rate of mammalian mitochondrial genomes. *J. Mol. Evol.* **48**, 427–434 (1999).

68. Riginos, C., Hickerson, M. J., Henzler, C. M. & Cunningham, C. W. Differential Patterns of Male and Female mtDNA Exchange Across the Atlantic Ocean in the Blue Mussel, *Mytilus edulis*. *Evolution (N. Y).* **58**, 2438–2451 (2004).

69. Wayne, R. K. *et al.* Molecular Systematics of the Canidae. *Syst. Biol.* **46**, 622–653 (1997).

70. Rawson, P. D. & Hilbish T.J. Asymmetric introgression of mitochondrial DNA among European populations of Blue Mussels (*Mytilus* spp.). *Evolution (N. Y).* **52**, 100–108 (1998).

71. Kijewski, A., Zbawicka, M., Vaïnoïa, R. & Wenne, T. K. Introgression and mitochondrial DNA heteroplasmy in the Baltic populations of mussels *Mytilus trossulus* and *M. edulis*. *Mar. Biol.* (2006). doi:10.1007/s00227-006-0316-2

72. Burzyński, A., Zbawicka, M., Skibinski, D. O. F. & Wenne, R. Evidence for recombination of mtDNA in the marine mussel *Mytilus trossulus* from the Baltic. *Mol. Biol. Evol.* **20**, 388–392 (2003).

73. Burzynski, A., Zbawicka, M., Skibinski, D. O. F. & Wenne, R. Doubly Uniparental Inheritance Is Associated With High Polymorphism for Rearranged and Recombinant Control Region Haplotypes in Baltic *Mytilus trossulus*. *Genetics* **174**, 1081–1094 (2006).

74. Stuckas, H., Stoof, K., Quesada, H. & Tiedemann, R. Evolutionary implications of discordant clines across the Baltic *Mytilus* hybrid zone (*Mytilus edulis* and *Mytilus trossulus*). *Heredity (Edinb).* **103**, 146–156 (2009).

75. Cao, L., Kenchington, E. & Zouros, E. Differential Segregation Patterns of Sperm Mitochondria in Embryos of the Blue Mussel (*Mytilus edulis*). *Genetics* (2004). doi:10.1534/genetics.166.2.883

Supplementary captions

Figure S1. *Mytilus trossulus* hemocytes cultivated for 24 hours. Cells were stained with TRITC-labeled phalloidin (red), and the nuclei (chromatin) were stained by DAPI (blue). Hemocytes of a healthy individual V1 (**a**) and a diseased individual J181 (**b**) were stained with tubulin primary antibodies, hemocytes of a diseased individual J54 (**c**) were stained with PCNA antibodies (green). Arrows in pictures of V1 point to actively moving cells, while arrowheads point to adherent cells. Star in picture of J54 marks the cell positive for proliferation.

Figure S2. Fragment analysis of *Mg*µ3 microsatellite locus from the hemolymph and the foot tissues of eight healthy mussels (control) and four DN-suggested mussels. Colored triangles designate putatively host-derived *Mg*µ3 fragments (green), putatively cancer-derived *Mg*µ3 fragments (violet); open triangles mark unrecognized fragments. The patterns of *Mg*µ3

764 fragments in the hemolymph and the foot tissues coincide in healthy mussels; an additional peak
765 is present in the hemolymph of DN-suggested mussels.

766 Figure S3. TCS network representing EF1α sequences obtained by molecular cloning. Sequences
767 from individual mussels and from different tissues (hemolymph and foot) are color-coded (see
768 legend on the top). All minor sequences represented by a single bacterial colony have been
769 removed.

770 Figure S4. *M. trossulus* and BTN COI haplotype network from the TCS analysis of 542-bp
771 alignment of 843 sequences. The data come from a reanalysis of the results (Fig. 5) with
772 additional 493 sequences from Crego-Prieto et al. (2015). Each circle represents a single allele.
773 The size of the circle is proportional to the number of individuals found to bear the allele. Bars
774 indicate mutations between alleles. Small black circles indicate hypothetical haplotypes
775 predicted by the model. The alignment is available as Supplementary Data S5.

776 Figure S5. (**a**) 479 bp long alignment subjected to recombination essay in RDP4 package with
777 default parameters included CR alleles of cancerous mussels detected in this study and in the
778 study of Yonemitsu et al. (2019), CR of 62mc10 individual from the Baltic Sea and the set of
779 reference male and female CR (see Accession numbers in the alignment included as
780 Supplementary data S6). The RDP4 package detected two recombination events in the region
781 around 249-263 nucleotide position of alignment in CR-D, D1, D2, D3, 1, 1‘ and 62mc10 and in
782 the region of 333-360 nucleotide position in CR-C, C1 and 2. RDP4 output p-values (cutoff of
783 0.05) are represented in the table. (**b**) The putative breakpoints marked at schematically depicted
784 alignment of CR used in the recombination analysis. Each bar represents a sequence. Pink color
785 designates standard F-mtDNA, blue color, standard M-mtDNA. The putative breakpoints are
786 marked with black vertical lines, designated by the nucleotide position from the start of
787 alignment. Sperm transmissible element is marked with a grey box.